IN-24
47949
P-25

NASA Contractor Report 195441

Thermomechanical Fatigue Behavior of Three CFCC's

Dennis W. Worthem
NYMA Inc.
Engineering Services Division
Brook Park, Ohio

N95-25880
Unclas
G3/24 0047949

(NASA-CR-195441) THERMOMECHANICAL FATIGUE BEHAVIOR OF THREE CFCC'S Final Contractor Report (NYMA) 25 p

March 1995

Prepared for
Lewis Research Center
Under Contract NAS3–25266

National Aeronautics and
Space Administration

THERMOMECHANICAL FATIGUE BEHAVIOR OF THREE CFCC'S

D.W. WORTHEM
NYMA, Inc.
Lewis Research Center Group
Brook Park, Ohio

Abstract

The thermomechanical fatigue (TMF) behavior of three continuous-fiber ceramic composites (CFCC's) was examined. The three matrices consisted of two different glass-ceramics and silicon carbide, respectively. The matrices of some of the specimens with the silicon carbide matrix were enhanced to improve oxidation resistance. All three were reinforced with Nicalon™ fibers with various fiber architectures. The thermoelastic properties of the matrix relative to the fibers, the elastic moduli and coefficients of thermal expansion (CTE), were different in each composite, providing a comparison of the effects of these critical properties. The specimens were tested under in-phase (IP) and out-of-phase (OP) cyclic loadings with respect to thermal cycling between 600°C and 1100°C.

One of the glass-ceramic composites had greatly increased TMF lives compared to the other glass-ceramic matrix composite. This was probably caused by the reversal of the CTE mismatch between the fibers and the matrices and caused by the different oxidation resistances of the composites. For the same TMF lives a cross-ply reinforced composite had a maximum cyclic stress half as great as that of a unidirectionally reinforced composite. This indicated that the [0°] ply fibers had a strong influence on TMF life. Both the glass ceramic matrix composites had shallow-slope stress-life plots that indicated sensitivity to damage and therefore low damage tolerance.

The composites with and unenhanced silicon carbide matrix experienced the shortest TMF lives of all the CFCC's tested. However the enhanced composite had the longest. Also, the enhanced composite demonstrated the best damage tolerance as evidenced by a stress-life curve that curves sharply upward to the left.

In all the composites, out-of-phase cyclic loading was worse than in-phase cyclic loadings despite the CTE mismatch between fiber and matrix. A damage investigation and a preliminary analysis of the stresses in the fibers and matrices taking into account their respective thermoelastic properties provided insight into the relative behavior of the glass-ceramic matrix composites under IP and OP TMF.

Introduction

Continuous-fiber ceramic composites (CFCC's) reinforced with fibers are proposed for high temperature components that will be subject to complex thermomechanical histories. In order to evaluate various CFCC's for these applications, testing will be required to simulate these histories in a simplified way. Thermomechanical fatigue (TMF) testing has been used to accomplish this for monolithic metals and has been extended to new metal and intermetallic matrix composites [1,2]. It is of interest to extend this testing to CFCC's. TMF behavior of CFCC's will be affected by several variables. External variables can be any conditions imposed by the experimental apparatus. These include the effect of the phase angle between load and temperature, the frequency and shape of the waveforms, the effect of the environment (for example, air versus argon).

Another external variable would be specimen design. Specimen design should avoid stress concentrations that cause failure away from a uniformly heated and stressed region. Specimen thickness may affect crack propagation rate and therefore TMF lives.

Internal variables are fiber architecture and composite constituent properties. Fiber architecture can be composed of layups of unidirectional plies, or of weaves and braids. The relative coefficients of thermal expansion (CTE) can change the stresses in the constituents of the composite and thereby alter TMF lives. Improvements in the oxidation resistance of CFCC's will come about through advances in constituent properties and composite processing. TMF testing will also allow the identification of damage mechanisms that provides insight for physically-based life prediction models. Composite properties and behavior may vary because of variation in the manufacturing process.

This study reports the results of exploratory TMF testing on three model-CFCC systems that examined the effects of the above mentioned variables. Two of the systems consisted of glass-ceramic matrices and the third had a ceramic matrix.

The two glass-ceramics had matrices with CTE's lower or higher than that of the fibers. One glass-ceramic system also had an altered matrix to improve oxidation resistance. A woven SiC/SiC composite with and without an altered matrix provided a composite with a minimal CTE mismatch. The mismatch however has not been measured. The only other reported TMF tests conducted on a CFCC were limited to one set of loading and temperature conditions and were not tested to failure [3].

Experimental Procedure

(1) Composites Materials

All the matrices were reinforced by ceramic-grade Nicalon™ fibers with a fiber volume fraction of about 0.39. The 10-15 microns (μm) diameter fibers were nominally silicon carbide and will be designated SiC throughout the remainder of this paper. Of the three matrices tested, two were glass-ceramics and one was a ceramic. The glass-ceramic composites were fabricated by hot-pressing followed by ceraming of the composites by a thermal process. One glass-ceramic was a calcium aluminosilicate glass-ceramic and the other was a magnesium aluminosilicate designated CAS-II and MAS-5, respectively. The designation "-II" indicates a second generation of the matrix and "-5" indicates the matrix was doped with 5% volume fraction of a borosilicate glass. Doping the matrix permits diffusion of boron to partially modify the pyrolytic carbon at the fiber/matrix interface for increased oxidation resistance and interfacial shear strength. Increasing the interfacial shear strength increases the microcracking stress of the composite [11]. The silicon carbide matrix was chemically vapor infilitrated (CVI) into the fiber preform. Silicon carbide is also chemically vapor deposited onto the composite panels to cover the residual porosity. The CVI silicon carbide matrix was also supplied enhanced by a proprietary process to increase the oxidation resistance of the composite.

Composite panels measured 15.6 centimeters (cm) x 15.6 cm. Unidirectionally reinforced CAS-II was 18 and 35 plies thick (nominally 0.3 cm and 0.6 cm, respectively). Unidirectional and crossply MAS-5 matrix composite panels were supplied 16 plies (nominally 0.3 cm) thick. Plain woven laminates of the silicon carbide composites were supplied 12 plies (nominally 0.35 cm) thick. Composite designations are SiC/CAS$[0°]_{18}$ and $[0°]_{35}$; SiC/MAS-5$[0°]_{16}$ and $[0°/90°]_{8S}$; SiC/SiC$[PW]_{12}$ (PW = plain woven laminates). The first three were produced by Corning, Inc. and the fourth by the DuPont Company. The manufacturers indicated that the glass-ceramic matrix composites had a porosity of about 1% and the enhanced and unenhanced SiC/SiC about 8-12%. Table I shows the properties of the matrices and fiber used. Properties of the CVI silicon carbide are not available but could be assumed close to the values for monolithic silicon carbide.

TABLE I-FIBER AND MATRIX PROPERTIES

Constituent	Room Temperature Young's Modulus, E, GPa (E_z for fiber)	600° C Young's Modulus, E, GPa (E_z for fiber)	1100°C Young's Modulus, E, GPa (E_z for fiber)	Poisson's ratio, ν, (ν_{zr} for fiber)	CTE, α, 10^{-6} m/m/°C, (α_{zr} for fiber)
Nicalon™ Fiber [Dow Corning, Inc.]	200	179	152	0.25	4.0
CAS-II matrix, Corning, Inc.	98	90	90	0.25	5.01
MAS-5 matrix, Corning, Inc.	138	unavailable(138)	unavailable(138)	0.25	2.4

(2) Load frame and instrumentation

The tests were conducted on a servohydraulic load frame with an axial load capacity of ±100 kN. The load cell has a dynamic rating of ± 25 kN. The unit has a fully digital control system which in turn was controlled by a personal computer. Strain measurements were made on an edge of the specimens by a capacitance type extensometer with a low contact force adjustment. The grips are the rigid, side-entry wedge type and are water-cooled. An alignment procedure was followed that attained bending strains within ± 60 microstrain at zero load in a strain-gaged tensile specimen that was 15.3 cm long, 1.27 cm wide, and 0.6 cm thick. The grips used for this study did not allow an improvement over these values of bending strains.

The grips and extensometer are enclosed in an environmental chamber that permited testing with flowing argon at a positive pressure. An inductively heated silicon carbide susceptor was used to heat the test specimen by radiation. Temperature was measured by Type R thermocouples routed through the endcaps of the susceptor and held against the specimen surface. Figure 1 is a schematic of the susceptor. Compressed air and argon were used for forced cooling during the cooling portion of the TMF cycles.

(3) Specimen dimensions

Specimen dimensions used for all the specimens were as shown in Fig. 2 except for those made of the SiC/CAS$[0°]_{35}$ and the enhanced SiC/SiC. The 41.9 cm radius in the transition region between the end region

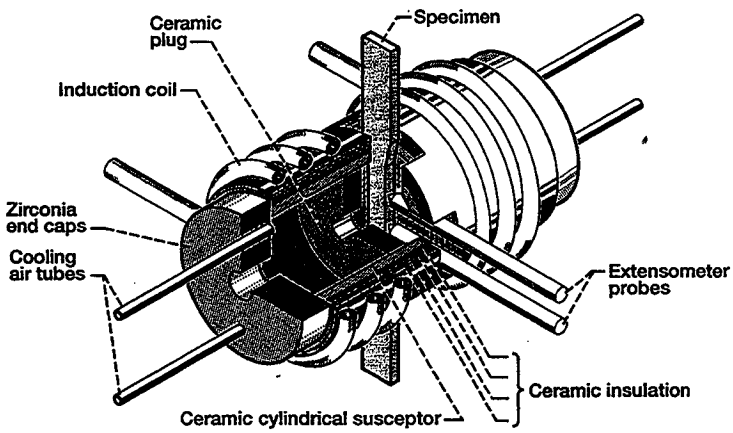

Figure 1 Susceptor design used with a 10 kW induction heater capable of heating ceramic matrix composites to 1650°C.

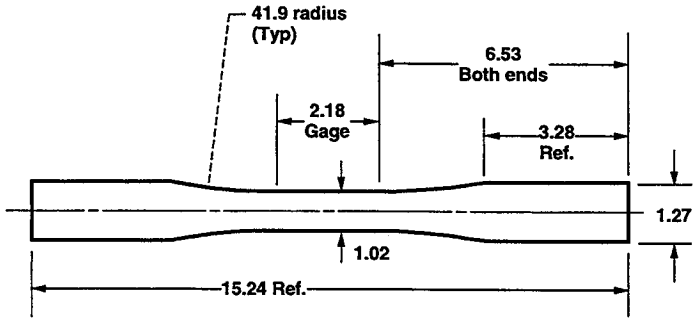

Figure 2 Dimensions in centimeters of the reduced gage section specimens. The transition region radius was either 36.8 cm or 41.9 cm. Thickness was as furnished.

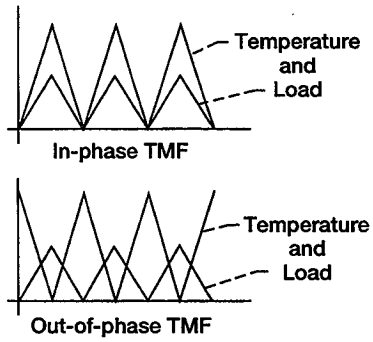

Figure 3 Schematics of load and temperature waveforms with zero-tension load control.

and the straight-sided gage section was chosen as a result of previous finite element analyses [4]. The analyses determined that this radius would minimize the possibility of failures in the transition region. The SiC/CAS$[0°]_{35}$ specimens had a similar design as in Fig. 2 but with a 36.8 cm radius and a 2.59 cm long gage section. Test results indicated no difference in behavior using a 36.8 cm or 41.9 cm radius. No tabs were used with the 0.6 cm thick specimens because they were thick enough (0.6 cm) to fit in the grips. Also, the stresses in the grip region are lower in a fatigue test compared to a tensile test. The other specimens used carbon fiber reinforced polyimide resin tabs which provided adequate high temperature capability. Specimens of the enhanced SiC/SiC were provided as machined by the composite manufacturer. The dimensions were, gage width of 0.9 cm, gage length of 4.0 cm, transition radius of 3.0 cm, grip region width of 1.25 cm, and total length of 20 cm.

(4) Test Conditions

Thermomechanical fatigue tests were conducted with a temperature range from 600°C to 1100°C. Above 1100°C in air the fibers were expected to degrade rapidly. Below 600°C, the control of cooling rates is difficult. The waveforms were

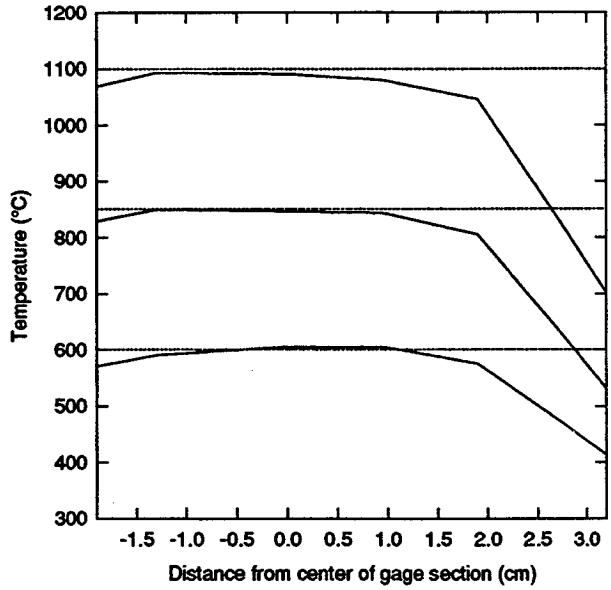

Figure 4 Temperature profile along the specimen when the gage section center is held at 1100°C, 850°C, and 600°C.

triangular with a six minute period. Tests were conducted in both air and argon. The stress ratio (minimum stress/maximum stress) was zero in all tests. The load was either in-phase or 180° out-of-phase with the temperature. Figure 3 shows schematically the load and temperature waveforms. Strains were measured during the tests to compare and contrast the deformation response of the model CFCC's to the two types of phasing [1].

Additional isothermal fatigue and creep tests were performed for comparison with the thermomechanical fatigue behavior. In the case of the isothermal fatigue tests the waveforms were triangular with a period of five minutes and a stress ratio of zero. The stress rupture time for the creep test is provided as an equivalent number of isothermal fatigue cycles to failure.

All tests, thermomechanical fatigue, isothermal fatigue, and creep were run to failure (complete separation into two pieces) or were interrupted at approximately 1000 cycles. Table II summarizes the test conditions used with each composite.

TABLE II-SUMMARY OF COMPOSITES AND TEST CONDITIONS
{Air environment and 600-1100°C unless otherwise stated}

Composite	Type of Test	Maximum stress, MPa
SiC/CAS[0°]$_{35}$	IP	150(2), 125 (2), 119.4, 74
SiC/CAS[0°]$_{35}$	OP	150, 125, 100, 72, 60, 50
SiC/CAS[0°]$_{35}$	IP (argon)	275
SiC/CAS[0°]$_{35}$	OP (argon)	250
SiC/CAS[0°]$_{35}$	ISO, 600°C	150
SiC/CAS[0°]$_{35}$	ISO, 1100°C	150, 136.8
SiC/CAS[0°]$_{35}$	Creep, 1100° C	150
SiC/CAS[0°]$_{18}$	IP	150(4), 125(2)
SiC/CAS[0°]$_{18}$	OP	125(2), 95, 80(2),70, 65(3)
SiC/MAS-5[0°]$_{16}$	IP	210(2), 175, 150
SiC/MAS-5[0°]$_{16}$	OP	210, 175(2), 165, 155, 150(2)
SiC/MAS-5[0°]$_{16}$	CS 600°-1100°C	210(2), 175
SiC/MAS-5[0°]$_{16}$	ISO, 23°C	210
SiC/MAS-5[0°/90°]$_{16}$	IP	150, 125, 100
SiC/MAS-5[0°/90°]$_{16}$	OP	150, 100, 75
SiC/SiC[PW]$_{12}$	IP	75, 65, 60, 55, 50(3)
SiC/SiC[PW]$_{12}$	OP	75(2), 65, 50, 40, 30
SiC/SiC[PW]$_{12}$	ISO, 600°C	65
SiC/SiC[PW]$_{12}$	ISO, 850°C	65
SiC/SiC[PW]$_{12}$	ISO, 1000°C	65
SiC/SiC[PW]$_{12}$	ISO, 1100°C	65, 50
SiC/SiC[PW]$_{12}$	Creep, 1100° C	65, 50
Enhanced SiC/SiC[PW]$_{12}$	IP	100
Enhanced SiC/SiC[PW]$_{12}$	OP	150, 125, 100, 85

Figure 4 shows the measured temperature profile along the specimen centerline when the center of the specimen gage section was held at 1100°C, 850°C, and 600°C. The temperature was within ±10°C of the target temperature in the gage section. The finite element analyses of reference no.4 was performed with this temperature profile and the thermoelastic properties of the composites. There is a small load-direction stress concentration of approximately 14 MPa along the edge of the specimen immediately outside the straight-sided gage section. However, the average stress across the specimen at this point is still less than that in the straight-sided gage section. If the composites maintain nonlinear deformation behavior because of microcracking with fiber bridging or creep, the stress should redistribute to still cause failure in the straight-sided gage section. However, environmental sensitivities at lower temperatures than in the gage section will cause failures where the maximum thermal stresses first cause microcracking.

(5) Materialography

Materialography was performed to allow investigation of the damage mechanisms in failed samples by optical and scanning electron microscopy. These CFCC's were extremely sensitive to cracking by the grinding and polishing procedures employed. After considerable experimentation a procedure was developed that produced consistent and reliable results.

Materialographic specimens were sectioned using a 152 μm thick diamond wafering blade. Six specimens, 6.4 millimeters (mm) long and half the test specimen-width wide, were cut transverse (perpendicular)to the load direction every 6.4 mm. The cuts spanned a total of 38 mm along the test specimen length from the straight-sided gage section through the transition region. Adjacent to the transverse sections two specimens 19 mm long were polished to a surface approximately midway through the test specimen thickness, longitudinal to the fibers and parallel to the width direction.

All grinding and polishing was done with semi-automated polishing equipment using a pressure of 200 N for one or two specimens and a pressure of 400 N for more than two specimens. Initially, the specimens are ground with 15 μm and 6 μm

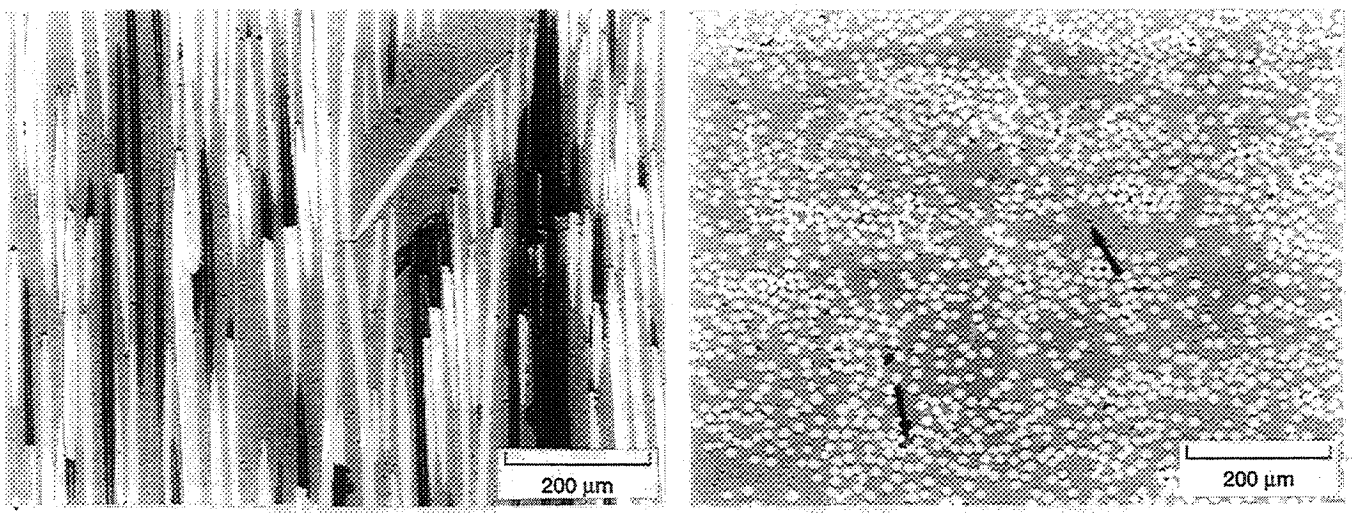

(a) (b)

Figure 5 Polished longitudinal (specimen width-horizontal direction), (a) and transverse (b) sections of SiC/CAS$[0°]_{35}$. diamond suspensions using copper-iron composite lapping disks. The polishing steps were by 6 µm and 3 µm diamond suspensions using plastic lapping disks, then 3 µm and 1 µm diamond suspensions using synthetic silk polishing cloths. Each step had a duration of nine minutes. The final step consisted of 0.5 µm diamond powder in a vibratory polisher using a long nap synthetic polishing cloth for approximately 18 hours.

Results and Discussion

(1) Materialography

Figures 5(a) and (b) show polished longitudinal and transverse sections of the SiC/CAS$[0°]_{35}$. No preexisting cracks were detected by optical microscopy up to a magnification of 1500X. However, there was considerable distribution of small pores (<10µm) and unfilled areas where fibers clump together (arrows).

Figure 6 shows a polished section of the SiC/MAS-5$[0°/90°]_{8S}$. The only preexisting cracks detected were short cracks in the matrix (requiring high magnification for observation) orientated radially from the fibers in the transverse section. Occasionally, these cracks occurred in groups in random areas. These cracks were not detected in the longitudinal section. Small pores (<10µm) were distributed throughout the matrix but were of a much smaller density than the SiC/CAS.

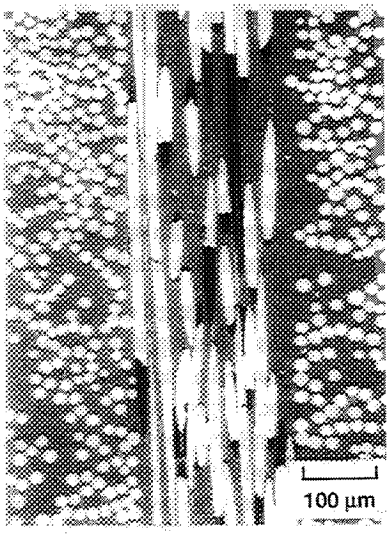

Figure 6 Polished transverse section of SiC/MAS$[0°/90°]_{8S}$ showing both plies.

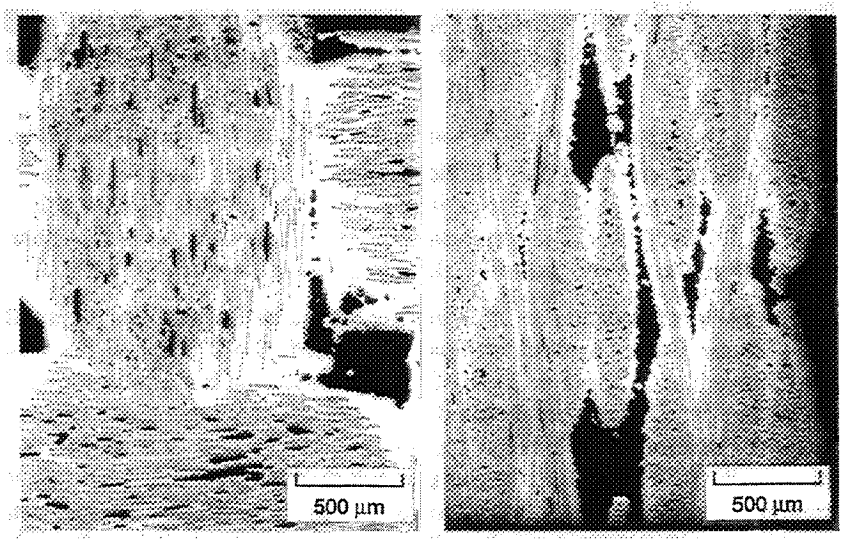

(a) (b)

Figure 7 Polished longitudinal (a) and transverse (b) sections of SiC/SiC$[PW]_{12}$.

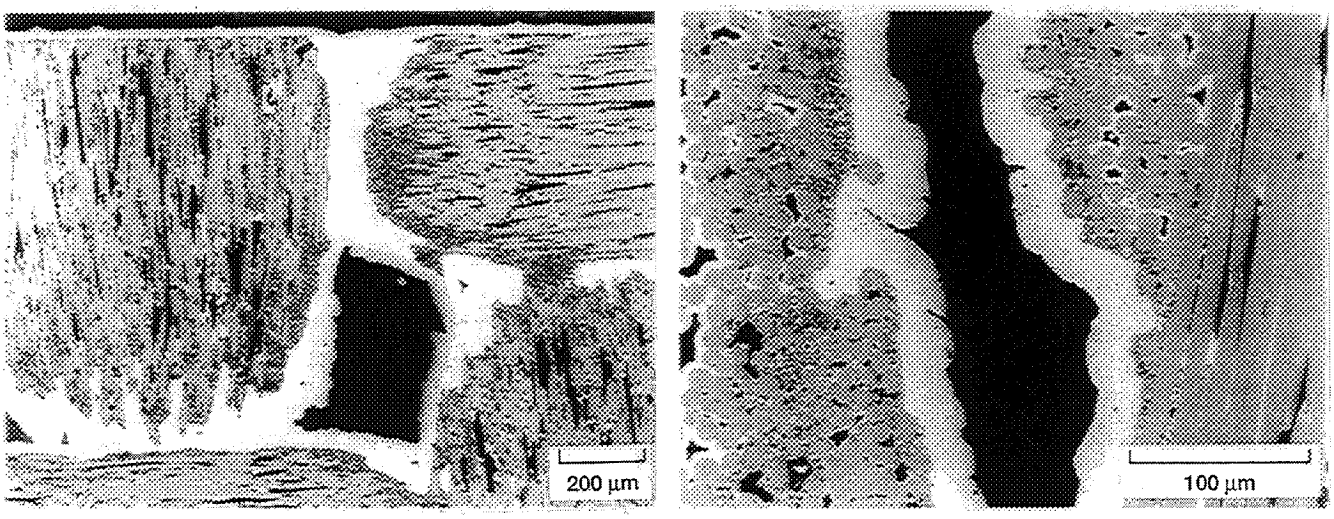

(a) (b)

Figure 8 Polished longitudinal (a) and transverse (b) sections of Enhanced SiC/SiC[PW].

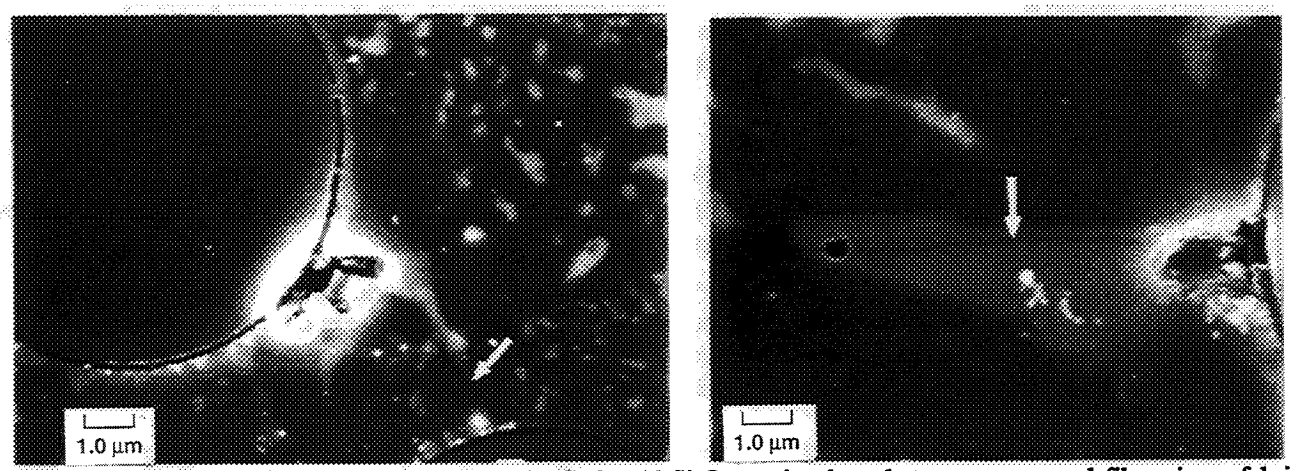

Figure 9 SEM micrographs of cracks (arrows) in Ca-Ba-Al-Si-O matrix phase between pores and fibers in as-fabricated SiC/MAS[0°].

Figures 7(a) and (b) show polished longitudinal and transverse sections of the unenhanced SiC/SiC[PW]$_{12}$. As reported by others [5] there were very large elliptically-shaped pores in the interbundle regions between fiber bundles. No preexisting cracks were detected by optical microscopy. Figures 8(a) and (b) show polished longitudinal and transverse sections of the enhanced SiC/SiC[PW]. The composite was essentially identical to the unenhanced composite except for the presence of particulates in the matrix, probably added to increase the oxidation resistance and fracture toughness of the matrix.

Since porosity is frequently an initiation site for fracture in ceramics [6], an SEM investigation was conducted of polished cross-sections from an as-fabricated piece of SiC/MAS-5[0°]. Figure 9 shows the presence of pores occuring in a distinct phase (lighter shade of gray). Most of the pores occurred in this phase. Additionally, this phase tended to surround the fiber perimeter. Cracks were detected in or near this phase that proceeded between pores or between a pore and a fiber. The crack plane appeared to be parallel to the load direction. It is not certain if these cracks were induced by the processing or the polishing. This composite was particularly difficult to polish because the MAS is relatively stiff and the glass-ceramics tend to have very low fracture toughnesses (~ 2 MPa-m^{½}). Occasionally, short cracks (<100 µm) proceeded from the pores in the SiC/SiC composites. These large pores (up to 0.5 mm^2) can be expected to have a major influence on the composite TMF behavior[5].

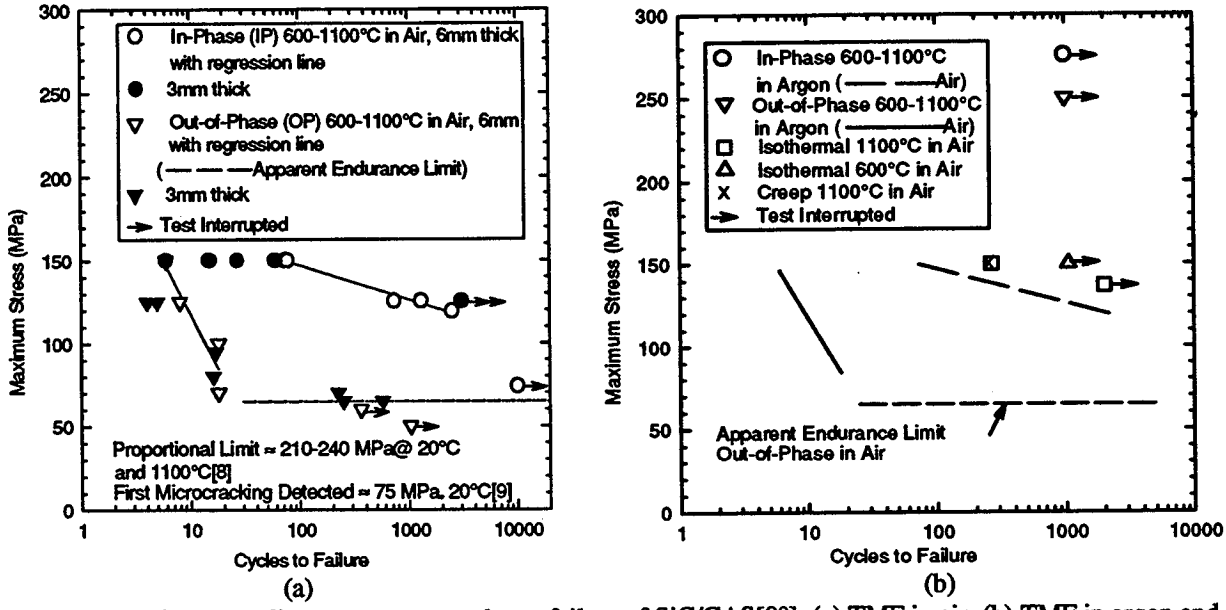

Figure 10 Maximum cyclic stress versus cycles to failure of SiC/CAS[0°]. (a) TMF in air, (b) TMF in argon and isothermal fatigue.

(2) Fatigue lives

(a) SiC/CAS

Figure 10(a) is a plot of maximum cyclic stress versus the log of cycles to failure for the TMF tests in air for the SiC/CAS$[0°]_{35}$ (6 mm thick). There were obvious differences in the TMF lives for the in-phase versus the out-of-phase loadings. At 150 MPa the life was 75 IP cycles versus 6 OP cycles, respectively, and at 125 MPa it was 1030 IP cycles versus 8 OP cycles. At 72 MPa the in-phase test was stopped at 10,176 cycles whereas the out-of-phase test failed on the 18th cycle. Below 72 MPa there was a dramatic increase in out-of-phase TMF lives (at approximately 65 MPa there was an apparent endurance limit). For both load phasings the failure points are well approximated with a straight line fitted by regression analyses. The apparent endurance limit was just below the 75 MPa that has been reported for detection of first microcracking in this composite system [7]. Also all the applied stress levels were well below the proportional limit of 210-240 MPa [8].

Figure 10(a) also plots the maximum cyclic stress versus the log of cycles to failure for the TMF tests with SiC/CAS$[0°]_{18}$. The 18 ply composite was approximately half as thick as the 35 ply composite. The results for tests with identical conditions as for the 35 ply composite are reported by the solid symbols. Both the OP and IP test results were similar to the thicker composite results. OP cyclic loading was considerably worse than IP cyclic loading. The only noticeable difference was in the IP results where a slope of a line drawn through the new data would be shallower than the old data. The thinner composite was probably better consolidated than the thicker, requiring a higher stress to initially propagate cracks, but the cracks would propagate faster at the same stress because of the thinner geometry. Normal fatigue scatter may also account for the difference.

Figure 10(b) compares the TMF tests in air with those in argon and with isothermal fatigue and creep tests in air. Only the lines determined from the regression analysis are repeated for the tests reported in Fig. 10(a). Tests were generally interrupted at

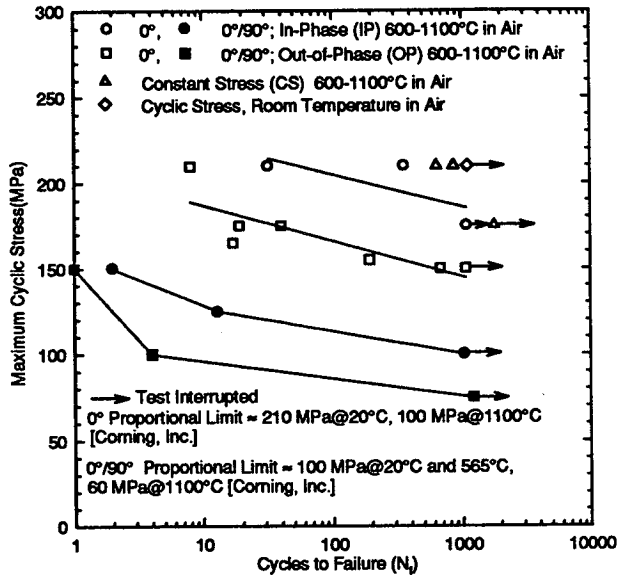

Figure 11 Maximum cyclic stress versus TMF cycles in air to failure of SiC/MAS$[0°]_{16}$ and $[0°/90°]_{8S}$.

approximately 1000 cycles for the two TMF tests in argon. The maximum cyclic stresses were 250 MPa and 275 MPa (both above the proportional limit for tensile testing in argon at 1100°C [8]) for in-phase and out-of-phase loadings, respectively. Fatigue failure at room temperature would probably occur in the grip before that in the gage section because finite fatigue lives are experienced around the room temperature proportional limit [9]. The isothermal fatigue life at 1100°C was 264 cycles but did not fail by 2005 cycles at 137 MPa. At 600°C and 150 MPa the test was stopped after 1000 cycles. The only creep test performed was at 1100°C and 150 MPa and failed in 25.4 hours or in 254 equivalent cycles. This was almost the same as the isothermal fatigue test at the same temperature and maximum cyclic stress. This implies that under isothermal conditions failure is determined by the time of exposure to the high temperature oxidizing conditions independent of whether the applied mechanical loading is constant or cyclic.

The results shown in Fig. 10(b) indicated a dramatic decrease in lives for TMF versus isothermal fatigue and creep in SiC/CAS. For this composite system the decrease was most dramatic for out-of-phase loading. Also the degrading effect of air was considerable.

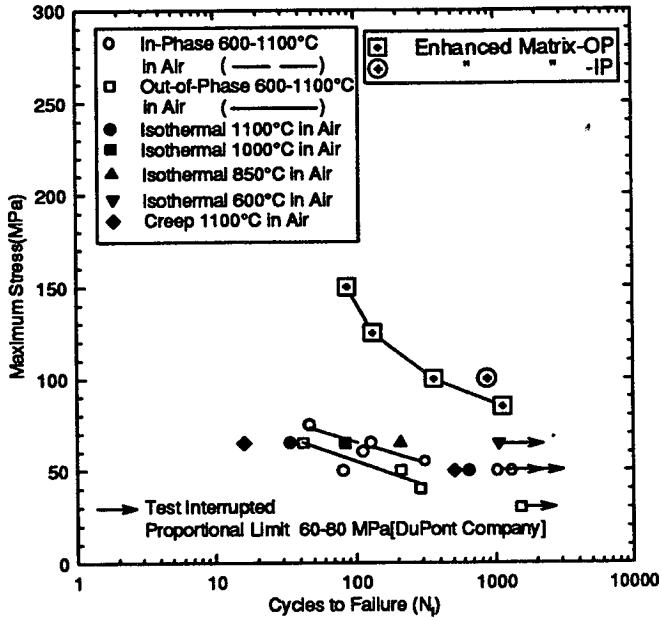

Figure 12 Maximum cyclic stress versus TMF cycles in air to failure of SiC/SiC[PW]$_{12}$ and. enhanced SiC/SiC[PW]$_{12}$

(b) SiC/MAS-5

Figure 11 compares the TMF tests for unidirectional and cross-ply SiC/MAS-5 in air under IP and OP cyclic loadings. For either fiber architecture OP TMF behavior was worse than IP. The applied maximum cyclic stress for the unidirectional composite was approximately twice that of the cross-ply for the same TMF life implying 0° ply fiber failure determined final composite failure. Slopes of the lines through the data points are relatively shallow. However, comparing the unidirectional behavior with that of the SiC/CAS in Fig. 10(a) indicated that there was a considerable improvement in TMF behavior over that of the SiC/CAS. The improvement is probably because of both the altered matrix and the different stresses in the constituents due to the changed CTE mismatch. In this composite, the TMF failures occur in the vicinity of the proportional limit during tensile testing.

Figure 11 also shows the results for two TMF tests performed with the stress held constant (CS). The two tested at 210 MPa failed but had longer lives than the IP tests at this maximum cyclic stress level. The fact that these tests lasted longer than either the IP or the OP tests indicates that cyclic loading is one determinant of TMF life. A result is also shown for a test that was cyclically loaded at room temperature. The test was interrupted at 1000 cycles in contrast to failures for the IP and CS TMF tests. This indicates that there was still a major effect of environment and CTE mismatch on this composite system.

TABLE III-MAXIMUM CYCLIC STRESS FOR A TMF LIFE OF 1000 CYCLES {Air environment}

	MAS-5[0°]	CAS[0°]	Difference
In-Phase	200	125	75
Out-of-Phase	150	65	85
Difference	50	60	
	MAS-5[0°]	MAS-5[0°/90°]	Difference
In-Phase	200	100	100
Out-of-Phase	150	75	75
Difference	50	25	
	Enh. SiC[PW]	SiC[PW]	Difference
In-Phase	100	50	50
Out-of-Phase	85	35	50
Difference	15	15	

(c) SiC/SiC

Figure 12 compares the TMF tests for plain woven SiC/SiC with and without an enhanced matrix in air under IP and OP cyclic loadings. For either matrix, out-of-phase TMF behavior was worse than in-phase. However, the enhanced matrix composite had a considerable improvement in TMF behavior. This is evidenced by both in a shift upward of the data and the fact that the enhanced data curves sharply upward at higher cyclic stresses that indicates improved damage tolerance. TMF failures for the unenhanced matrix composite

occurred at maximum cyclic stresses below the tensile proportional limit, whereas they were above the tensile proportional limit for the enhanced matrix composite.

(d) Summary of Fatigue Results

Tables A.1-A.6 in the Appendix summarizes the results of all tests performed on the three composites.

Table III provides the estimated maximum cyclic stress at which the TMF lives were approximately equal to 1000 cycles. The SiC/SiC composite with a matrix enhanced to improve oxidation resistance performed the best. Examining the difference of the rows and columns in Table III shows a number of interesting things. The differences in maximum cyclic stress between IP and OP for either unidirectional MAS-5 or CAS are approximately the same, 50 and 60 MPa, respectively. Also the differences in maximum cyclic stress between the two composites for IP or OP TMF are approximately the same, 75 and 85 MPa, respectively. This may indicate that the maximum cyclic-stress threshold for failure may be determined by analysis of the composites under the respective test conditions

The difference column on the right side of the middle section of Table III shows that for the MAS-5 matrix composites, the maximum cyclic stresses for the crossplies was half that of the unidirectional under either IP or OP TMF (100 versus 200 MPa and 75 versus 150 MPa). Since there was only half the number of fibers in the load direction, this implies that fatigue lives were determined by the failure of the 0° ply fibers. At the bottom this result is also demonstrated by the fact that the difference between IP and OP for the crossplies is only half that of the unidirectional. This result implies that the threshold may be determined by analysis of the thermomechanical behavior of the composite constituents.

The last section of Table III compares the threshold values of maximum cyclic stress for the SiC/SiC composites with and without enhanced matrices. The differences on the bottom are the same and the differences on the right are the same suggesting again that behavior occurred that is subject to analysis.

(2) Deformation Behavior

All three composites experienced similar deformation behavior. Figure 13 shows the maximum and minimum total (thermal and mechanical) strains as a function of cycles in a typical IP TMF test, respectively. After an initial transient response, the composite experienced cyclic ratcheting until failure occurred. The ratcheting rate decreased throughout the life. Butkus et al. [3] reported similar behavior. Under OP loadings the composite experienced zero ratcheting (constant strains) after an initial transient response. Throughout the tests the strain range remained essentially constant. In the longest tests, the ratcheting rate was near zero at large number of cycles (>2000). The strain range however, remained essentially constant throughout the test that was typical of all the fatigue tests reported in this paper. Only very close to failure (last few cycles) was there a major change in strains. Isothermal fatigue, and creep tests show behavior typical of the IP maximum cyclic strain in Fig. 13.

Also, there is no obvious correlation between the strain at failure and the number of cycles to failure. However, time and temperature-dependent deformation behavior is still important to accurately analyze the stress states of the fibers and matrix. This subject requires further study.

Measurement of the strains was complicated by the presence of forced cooling which produced transient behavior early in the TMF testing and to a lesser extent during each cycle throughout the tests. Future testing will require a test procedure that measures the CTE and Young's modulus at the minimum and maximum temperatures in the TMF cycle before the test is started and periodically during the test [10]. Additionally, ten thermal cycles should be applied at the beginning of the test to equilibrate the thermal cycle. Testing performed late in this set indicated no effect on TMF life from this initial thermal cycling.

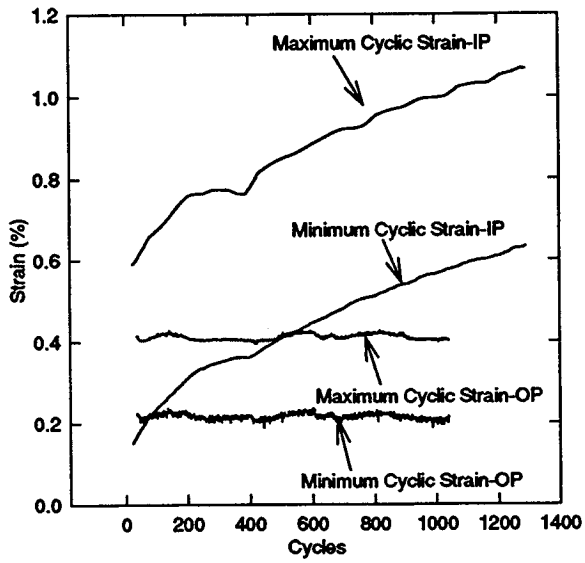

Figure 13 Maximum and minimum cyclic strains in typical IP and OP TMF tests, SiC/CAS$[0°]_{35}$; IP, σ_{Max}= 125 MPa, N_f = 1313; OP, σ_{Max}= 50 MPa, N_f = 1039.

(3) Failure locations and damage mechanisms

Figure 14 shows the typical failure locations in the specimens whether out-of-phase TMF, in-phase TMF,

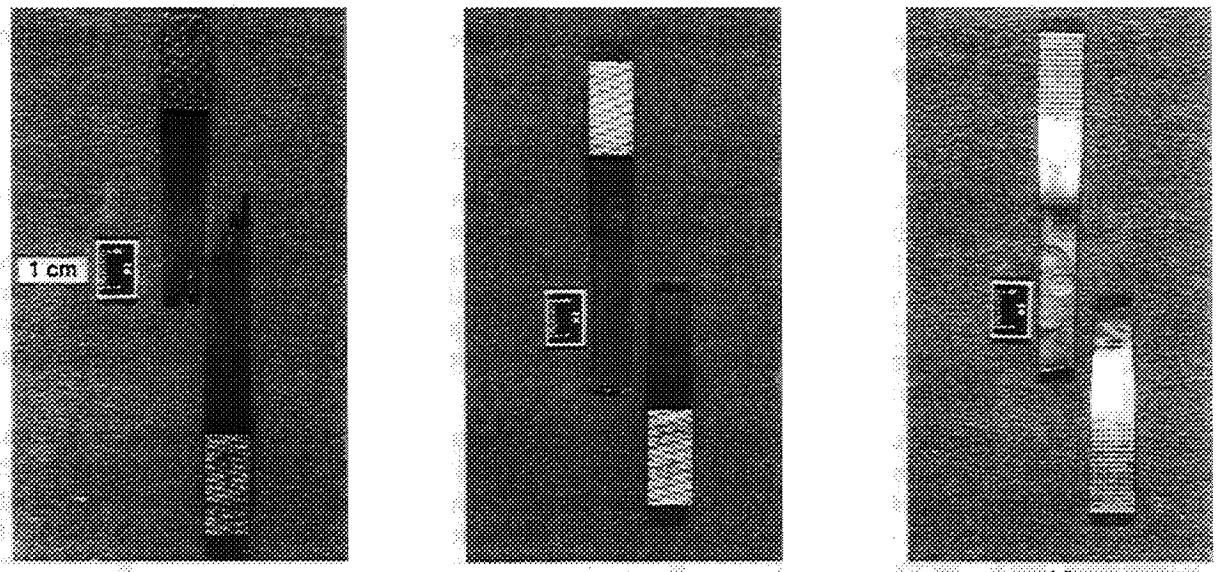

(a) (b) (c)

Figure 14 Typical failure locations in fatigued specimens. (a) OP TMF, SiC/MAS-5$[0°]_{16}$, σ_{Max}= 175 MPa, N_f = 40, (b) IP TMF, SiC/MAS-5$[0°/90°]_{8S}$, σ_{Max}= 125 MPa, N_f = 13, (c) OP TMF, SiC/SiC$[PW]_{12}$, σ_{Max}= 40 MPa, N_f = 288.

isothermal fatigue, or creep tests. Most of the specimens experienced final failure in either the upper or lower transition region rather than in the straight-sided gage sections. Only occasionally were the failures between the extensometer rods. Failure always occurred near or at the maximum applied cyclic stress. The fracture path tended to be very jagged in unidirectional composites but transverse to the load direction in the cross-ply and plain woven composites.

Tables A.1-A.7 in the Appendix also provide the failure location in each failed specimen and is summarized in Table IV for the TMF tests only. Table IV shows the average temperature and direct stress at the failure locations. The two temperatures shown are the temperatures at the failure locations when the gage section was at 1100° and 600°C, respectively. Tables A.1-3 that are for the unidirectionally reinforced glass-ceramics indicate that the OP specimens tended to fail very close to or inside the straight-sided gage-section. Since the failures occurred at or near the maximum cyclic applied stress, the failures occurred at about 600°C. However, the IP specimens all failed further from the gage section than the OP specimens, when the gage section temperature was about 1100°C and at the maximum cyclic applied stress. The temperatures at the failure location in the IP specimens were from 620° to 706°C, close to those for the OP specimens.

Table A-5 for the unenhanced plain woven SiC/SiC indicated that the OP specimens

TABLE IV-SUMMARY OF FAILURE LOCATIONS

(For the failure locations, U = upper half and L= lower half of specimens, G = within gage section.)

Table-IP or OP	Number failed above gage section	Number failed below gage section	Number failed in gage section U=upper half L=lower half	Temp, (°C) at average failure location when gage section at 1100°-600°C	Nominal stress (MPa) in loading direction at average failure location, (%) of gage section stress
A.1-OP	0	3	1L	1070-582	100
A.1-IP	0	5	0	648-385	90
A.2-OP	1	1	3U	1090-597	100
	2	2	0	764-437	92
A.2-IP	1	3	0	706-411	90
A.3-OP	0	0	3U,2L	1097-600	100
	0	1	0	961-527	97
A.3-IP	1	1	0	620-372	88
A.4-OP	1	1	0	1064-580	99
A.4-IP	1	1	0	1071-584	100
A.5-OP	2	2	1L	1073-580	99
A.5-IP	1	2	0	1062-576	99
	0	1	0	942-519	97
	1	0	0	855-479	95
A.6-OP	0	0	2U	1092-600	100
	0	0	1U	1031-560	100
	1	0	0	934-515	96
A.6-IP	1	0	0	988-540	99

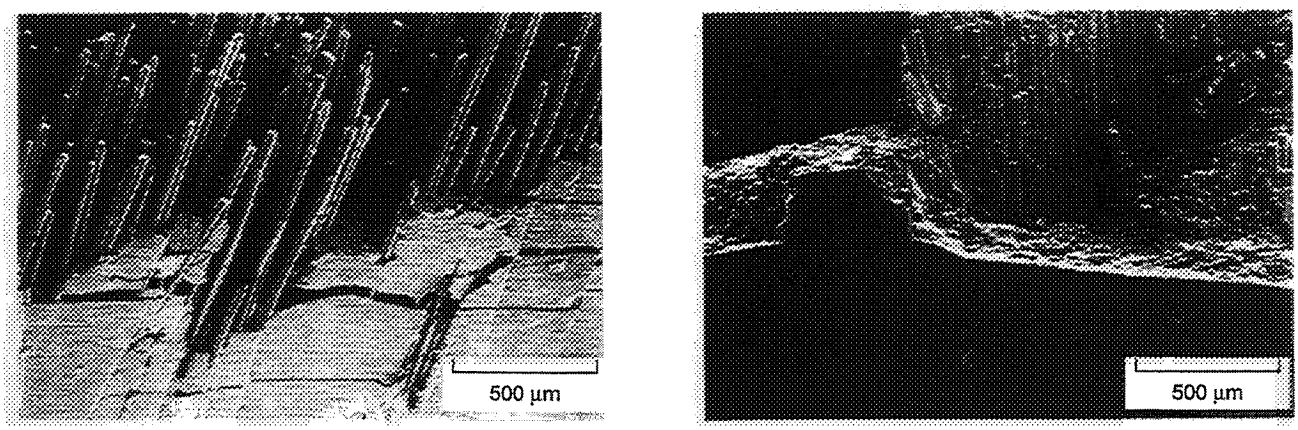

(a) (b)

Figure 15 SEM micrographs of typical fracture surfaces, (a) room temperature tension, (b) high temperature tension (SiC/CAS[0°]).

failed near the gage at 600° but the IP specimens experienced more random failure at various temperatures from 855° to 1062°C. There were too few data points in Tables A.4 and A.6 for the cross-ply reinforced glass-ceramic and the enhanced plain woven SiC/SiC, respectively to draw any inferences about those composites. Also, the smaller radius used for the enhanced SiC/SiC increased the stress concentration in the transition and may have strongly influenced the failure location.

The failure locations, at least for the unidirectionally reinforced glass-ceramics, indicated that the specimens fail at an intermediate temperature (600°-700°C) rather than at the maximum temperature (1100°C). This result was consistent for OP specimens in that the gage section was at 600° C when the applied stress was a maximum. However, for the IP specimens this result indicated that the composite was weaker or more brittle at the intermediate temperatures. At this temperature the matrix was probably still brittle but the carbon interface was subject to oxidation. The result was embrittlement of the composite. However, at 1100 C there was sufficient creep deformation of the matrix to retard cracking, thus protecting the composite from oxidation embrittlement. Two reasons are offered here why the OP specimens had a tendency to fail slightly inside the transition regions. One, residual concentric bending strains was at a maximum at these regions. Two, thermoelastic finite element analyses of the specimens treating the composites as homogeneous orthotropic materials revealed moderate local stress concentrations (14 MPa) as a result of the measured temperature gradient (Fig. 4) in this region. Since the composite was sensitive to oxidation embrittlement from any cracking, failures would occur at these stresses because the composite did not retain psuedo-ductility from fiber bridging and interface sliding. The last section will discuss the causes of failure in more depth.

(3) Damage mechanisms

Figure 15 shows scanning electron microscope (SEM) micrographs of SiC/CAS[0°]. The figure compares the failure surfaces of a room temperature tensile tests performed in an earlier study (ref. 5) and the typical failure surface of TMF or isothermal fatigue specimens. The failure surfaces did not appear to be significantly different between TMF and isothermal fatigue. The room temperature tensile test surface showed the same relatively flat fracture surface transverse to the fibers, fiber pullout and periodic matrix cracking typically experienced with fiber-reinforced CFCC's [8,11]. The high temperature fatigue tests showed flat fracture surfaces with almost no fiber pullout near the specimen surface but with jagged faceted features (almost longitudinal fracture surfaces) on the remainder of the fracture surface.

Figure 16 shows scanning electron microscope (SEM) micrographs of fracture surfaces for the SiC/MAS-5. Figure 16(a) and (b) compares the failure surfaces of IP and OP tests of cross-ply SiC/MAS-5, respectively. The IP failure surface had a small area (arrow) at one edge that was very flat with little fiber pullout. Fiber pullout was experienced in most of the remainder of the fracture surface. There was a much larger area of no fiber pullout on the OP failure surface indicating more oxidation embrittlement of the fibers and/or of the interfaces than in the IP specimens.

Figure 17 (a) and (b) shows SEM micrographs of the same two specimens as in Fig. 16 but at a much higher magnification. There was a small amount of fiber pullout in the IP specimens (Fig 17(a)), whereas there was essentially none in the OP specimens (Fig 17(b)). There were brittle fracture features on both the fibers and matrix. However, there was some flow of both, probably caused by exposure to the environment after the crack propagated through the areas shown in the figures.

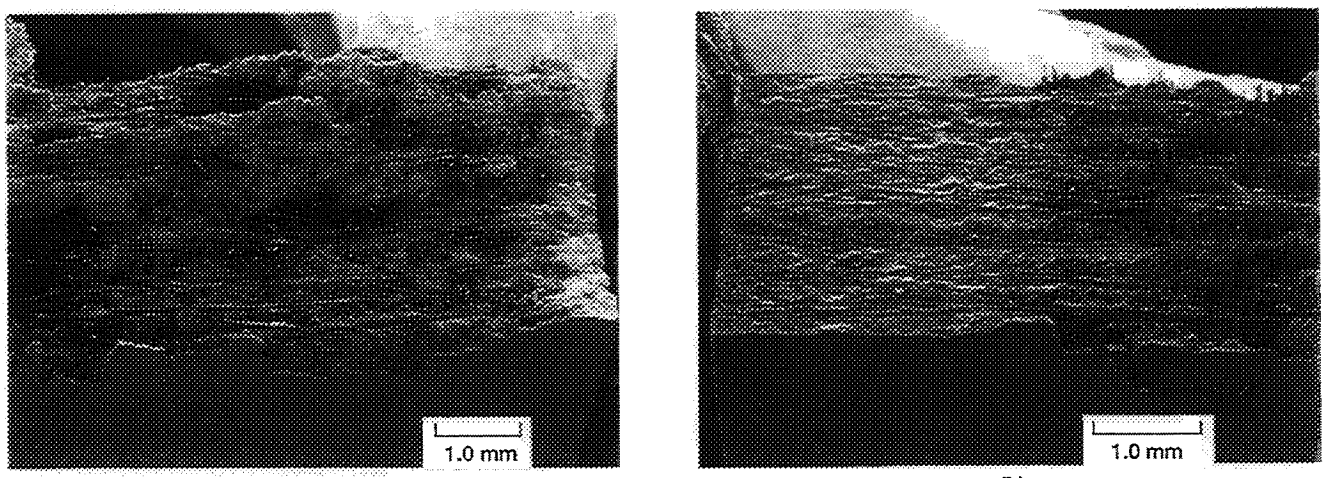

(a) (b)

Figure 16 SEM micrographs of typical fracture surfaces(a) IP TMF, SiC/MAS-5[0°/90°]$_{8S}$, σ_{Max}= 125 MPa, N_f = 13, (b) OP TMF, SiC/MAS-5[0°/90°]$_{8S}$, σ_{Max} = 100 MPa, N_f = 4.

The small areas in the IP specimens with no pullout (not shown here) were distinctly brittle as evidenced by steps on both the fiber and matrix fracture surfaces and sharp circumferential edges on the fiber fracture surfaces. These areas were presumably the areas of tensile overload at TMF failure. The specimens shown in Fig 17 had cross-ply architectures and the IP specimens failed near the gage section. However, the unidirectional SiC/MAS-5 composites tested in IP conditions had failure locations further into the transition region with fracture surfaces with no fiber pullout. It is not known why the cross-ply composites were more resistant to failure in the transition region, except that the specimens shown in Fig. 17 were tested at conditions that produced very short lives. If the cross-ply IP specimens were tested at slightly lower maximum cyclic stresses and lasted longer the failures may have occurred in the transition region.

Figure 18 compares the fracture surfaces of the plain woven SiC/SiC without and with an enhanced matrix. Fig. 18(a) was for an IP test with the unenhanced matrix and Fig. 18(b) was from an OP test with the enhanced matrix. The unenhanced composite had considerable bonding of the fiber bundles to the matrix indicating oxidation embrittlement. However, the enhanced composite retained pullout by the fiber bundles, indicating improved damage tolerance that agrees with the life data presented in Fig. 12.

Polished longitudinal and transverse sections from three failed specimens SiC/CAS[0°] were examined by optical microscopy to compare damage in OP, IP and IF tests. These specimens allowed the investigation of damage distinct from

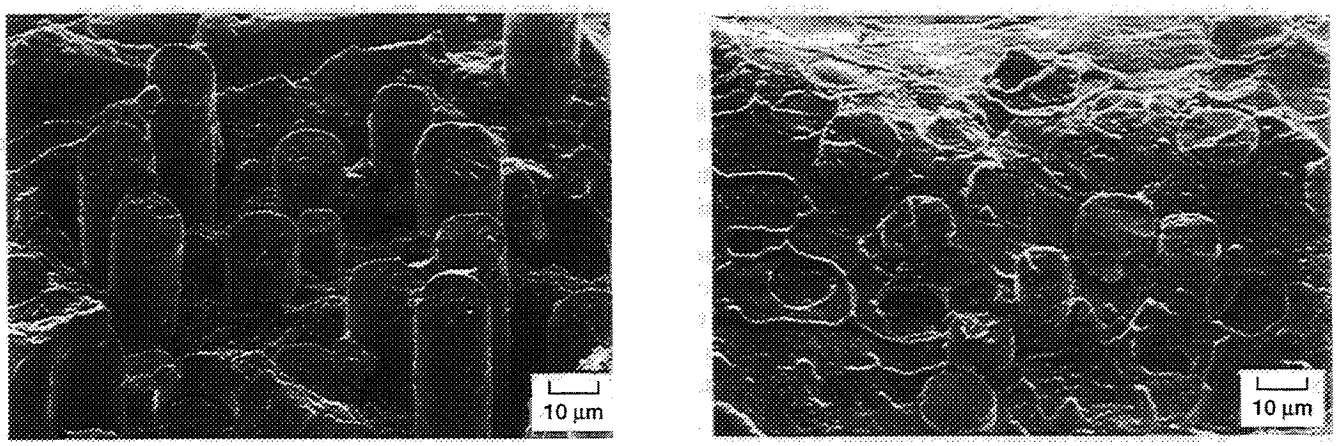

(a) (b)

Figure 17 SEM micrographs of typical fracture surfaces(a) IP TMF, SiC/MAS-5[0°/90°]$_{8S}$, σ_{Max}= 125 MPa, N_f= 13, (b) OP TMF, SiC/MAS-5[0°/90°]$_{8S}$, σ_{Max}= 100 MPa, N_f= 4.

the main failure crack. This damage would presumably be representative of the precursors of the final failure crack. The highest crack density and crack opening displacements were found in the OP loaded specimens. The IF specimens in contrast had very few such cracks. These trends were in agreement with the fatigue lives of the various thermomechanical histories. The longitudinal sections (Figs. 19 (a), (b), and (c)) show that a few transverse cracks in the matrix (distinct from the main failure crack) were present in the gage sections of both TMF tests but not in the IF test. The cracks proceeded from the edge (right side of photographs) into the specimen approximately 1-2 mm. However, as seen in Figs. 19 (a), (b), and (c), the residual crack opening displacement was greater in the OP test than the IP test. Also in the OP test the fibers were fractured in the crack plane, whereas in the IP test the crack was apparently fully bridged by fibers. There was no damage or cracking detected in the transverse sections. In the SiC/CAS[0°] specimens tested in argon, periodic matrix cracking was observed after the tests were interrupted. Distribution was similar to that in a tensile test [8,11].

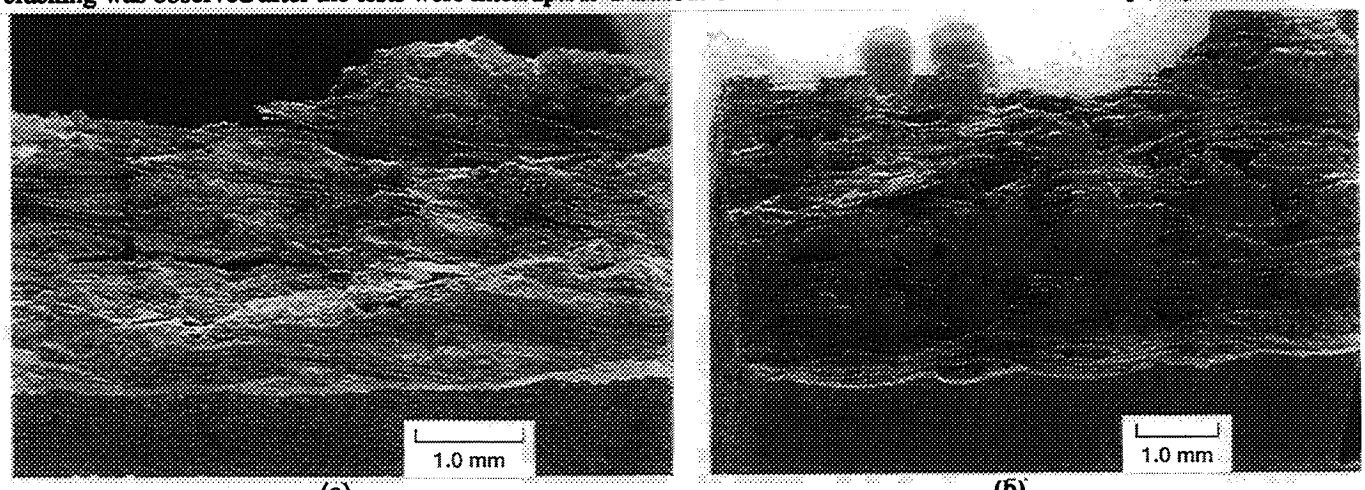

Figure 18 SEM micrographs of typical fracture surfaces(a) IP TMF, SiC/SiC[PW]$_{12}$, σ_{Max}= 40 MPa, N_f = 288, (b) OP TMF, Enhanced SiC/SiC[PW]$_{12}$, σ_{Max}= 125 MPa, N_f = 133.

Polished longitudinal (Figs. 20(a) and (b)) and transverse sections from failed specimens of the SiC/MAS[0°], [0°/90°], were also examined by optical microscopy. Longitudinal sections (Figs. 20(a), and (b)) of the SiC/MAS[0°] and [0°/90°] show that cracking occurred virtually the same as in the SiC/CAS[0°] (specimen edge on the left side). Also as in the SiC/CAS[0°], the fibers had fractured on the crack plane in the OP specimen but not in the IP specimen. The residual crack

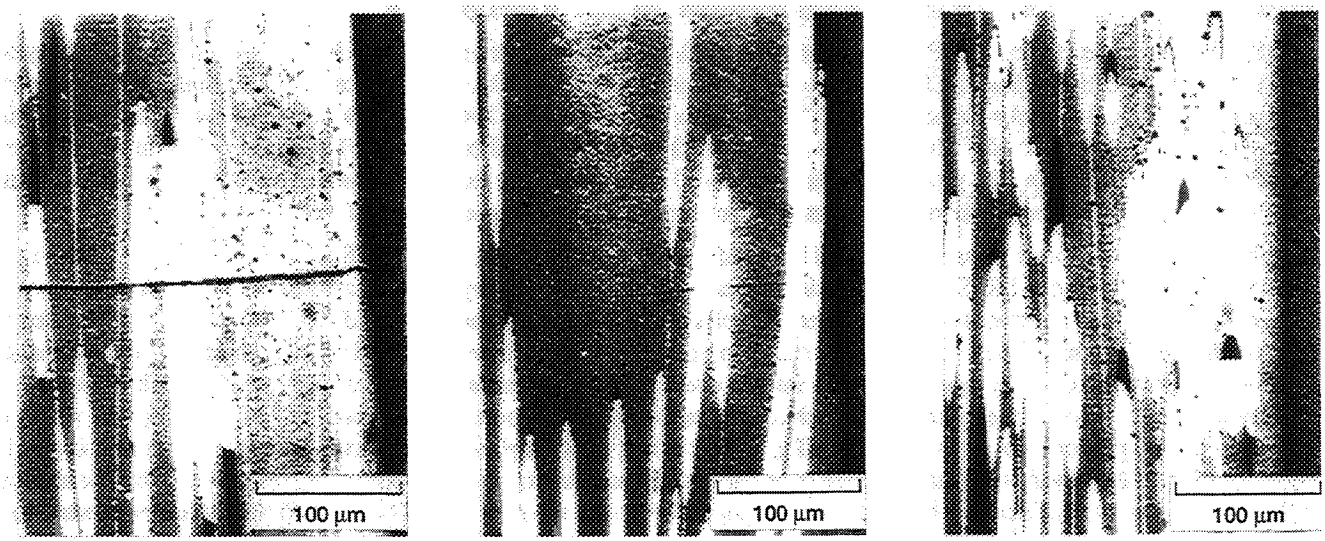

Figure 19 Optical micrographs, longitudinal sections. (a) OP TMF, 600°-1100°C, SiC/CAS[0°]$_{35}$, σ_{Max}= 150 MPa, N_f = 6, (b) IP TMF, 600°-1100°C, SiC/CAS[0°]$_{35}$, σ_{Max}= 150 MPa, N_f = 73, (c) IF, 1100°C, SiC/CAS[0°]$_{35}$, σ_{Max}= 150 MPa, N_f = 264.

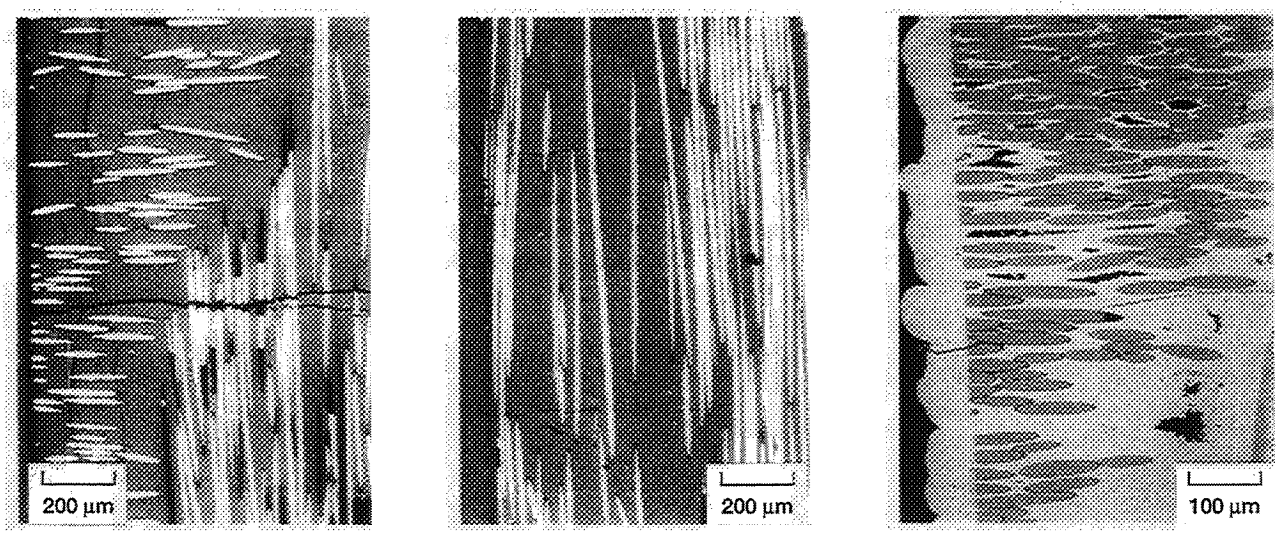

Figure 20 Optical micrographs, longitudinal sections. (a) OP TMF, 600°-1100°C, SiC/MAS-5$[0°/90°]_{8S}$, σ_{Max}= 100 MPa, N_f = 4, (b) IP TMF, 600°-1100°C, SiC/MAS-5$[0°]_{16}$, σ_{Max}= 175 MPa, N_R = 1072, (c) OP, TMF, 600°-1100°C, SiC/SiC$[PW]_{12}$, σ_{Max}= 40 MPa, N_f = 288.

opening displacement in the OP specimen was greater. The cracking parallel to the specimen edge in Fig. 20(a) was an artifact of the polishing procedure. The presence or lack of fiber bridging agrees with the SEM micrographs in Figs.16 (a) and (b). The OP fracture surface had a larger area of flat fracture surface (fibers broken on the crack plane) compared to the IP fracture surface that had a much greater extent of fiber pullout. In both glass-ceramic matrix composites, the matrix was apparently subjected to a more severe condition in the OP tests. This led to facilitated matrix fracture with a higher local stress transfer to the fibers and penetration of oxygen to these localized regions on the fibers. This was consistent with the oxidation of the interface causing a bonding of the matrix to the fiber, thereby increasing the local stress transfer to the fibers [15,16]. Microstructural degradation of the fibers by oxidation could have also contributed to the failure [13]. The last section will attempt to rationalize why the IP specimens had longer TMF lives for the same maximum cyclic applied stress and the failures occurred at locations with approximately the same temperature.

The SiC/SiC specimen tested in OP TMF shown in Fig 20(c) experienced transverse and longitudinal cracking in only one area of the cross-section where the final failure crack appeared in the opposite transition region. As in the glass-ceramic matrix composites, the cracks appearred to start from the edge and proceed inward. However, there was more meandering of the cracks between fibers and fiber bundles and the cracks interconnected between the large pores. The maximum cyclic stress of 40 MPa was below the proportional limit of 60-80 MPa where one expects isolated cracking in the matrix. This unenhanced composite was apparently very sensitive to microcracking and penetration of oxygen.

Figures 21 (a) and (b) show transverse (a) and longitudinal (b) sections of the enhanced SiC/SiC tested in OP TMF. In contrast to the unenhanced SiC/SiC, the cracking appeared periodically on any particular polished plane. At least one transverse (to the load direction) crack appeared in each interbundle region between bundles. The deflection of the cracks between bundles combined with the enhanced matrix presumably provides the improved damage tolerance in the enhanced SiC/SiC. Improved oxidation resistance at the interface and fracture toughness of the matrix probably result from the particulate matter added to the matrix. This behavior occurred at a maximum cyclic stress (125 MPa in Fig. 21) which was above the tensile proportional limit of 60-80 MPa. In this cyclic stress region, one expected more extensive matrix cracking behavior [5,11]. However, the enhanced matrix provided increased tolerance to the cracking compared to the unenhanced matrix. This was by evidenced by the higher cyclic stress levels and the shape of the curve in Fig. 12 (curves upward to the left).

Transverse cracking of the matrix in all the TMF tests apparently allowed oxygen to penetrate the composite and degrade the fibers and interface. The stresses in the matrix under TMF are determined by the thermoelastic and time-temperature

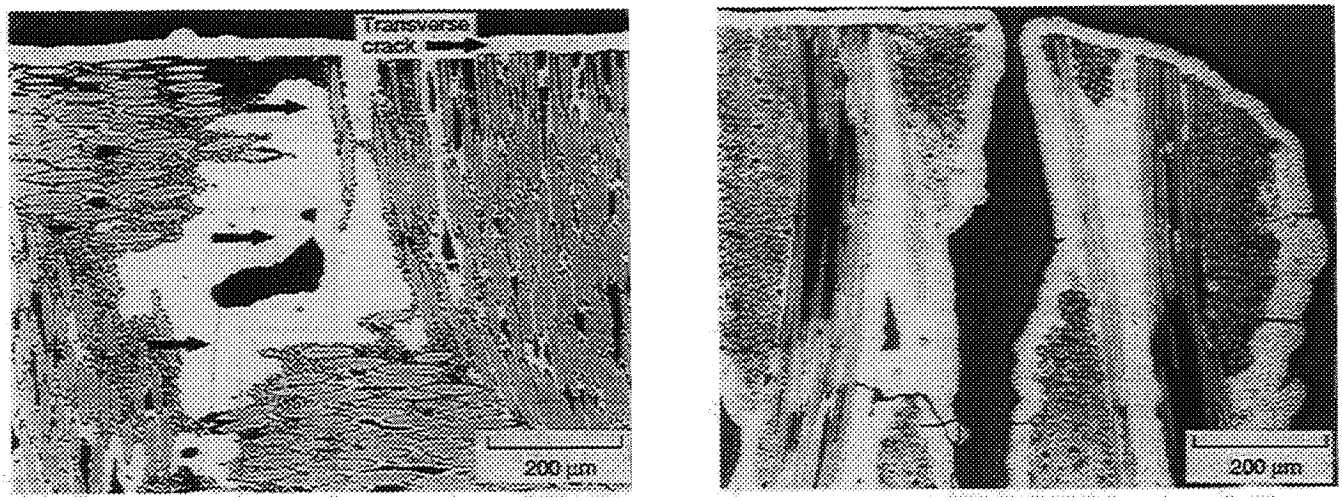

(a) (b)

Figure 21 Optical micrographs, (a) longitudinal section and, (b) transverse section. OP TMF, 600°-1100°C, Enhanced SiC/SiC[PW]$_{12}$, σ_{Max}= 125 MPa, N_f = 133.

deformation properties of the constituents. Presumably, the stress state in the matrix during OP testing would be worse than during IP testing.

(4) Constituent Stress Analysis

Insight into rationalizing some of the TMF results was provided by the damage mechanisms described in the last section. Figure 22 shows schematically cracks that initiated in the glass-ceramic and unenhanced silicon carbide matrix composites. The cracks initiated at or near the edge and propagated across the specimen width. The few cracks that developed usually occur toward either end of the straight-sided gage section. In the OP specimens this occurred closer to the beginning of the curved transition, but further into the transition region in the IP specimens. Failures seemed to occur at the combination of maximum applied stress and a temperature of 600-700° C except for the unenhanced SiC/SiC IP specimens whose failure locations were more random. The final failure crack usually developed from one of these edge cracks.

In the enhanced silicon carbide matrix composites, symmetric edge cracks developed periodically throughout the straight-sided gage section. The cracks appeared to initiate at the edges of the specimen and proceeded into the composite where interbundle regions were in proximity to the edge. As in the other composites the final failure crack developed from one of the edge cracks that initiated in either transition region. However, a much smaller radius and a larger width reduction were used in the specimen design for the enhanced SiC/SiC. This radius produced a larger stress concentration in the transition region at the end of the gage section. It is possible that failures for this composite would have also occurred under IP conditions further up in the transition region if the specimen design of Fig. 2 were used.

Presumably, the stresses that caused the edge cracks in the unidirectionally reinforced glass-ceramic composites can be

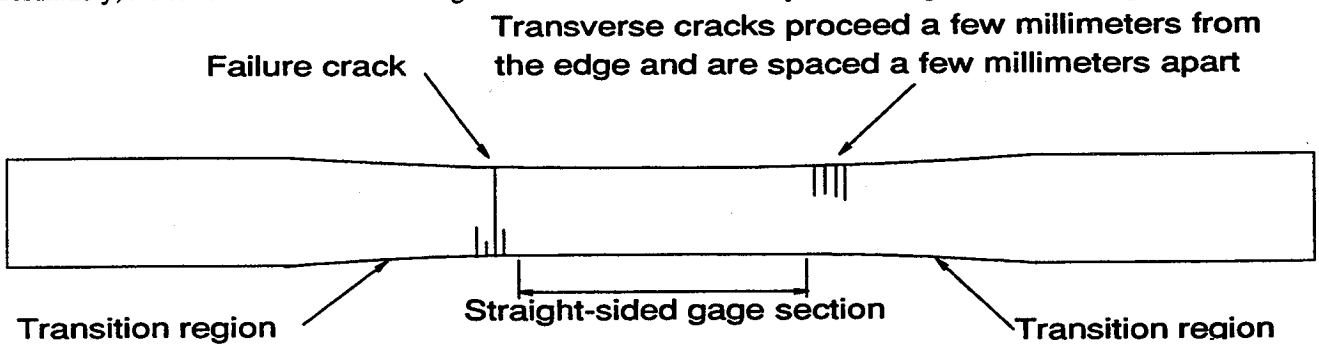

Figure 22 Schematic of typical cracks proceeding from edge of specimen.

determined from the mismatch of CTE's and elastic moduli of the constituents. A simple thermoelastic concentric cylinder model was employed for this study. Such stresses would of course only have existed for the first few cycles. This was because other factors such as relative time-temperature dependent deformation (referred to as creep in this paper for short) of the constituents or the presence of microcracking would have caused redistribution of stresses. However, because the TMF life behavior implied that the composites tested are very sensitive to the initiation of microcracking in the matrix, it was justified using a simple approach to investigating the stresses in the fibers and matrix under initial test conditions. In this section, the results of the TMF testing will be discussed in the context of the calculated thermoelastic stresses and the influence of creep and microcracking will be discussed qualitatively. More sophisticated models and interrupted tests will be required to provide further verification.

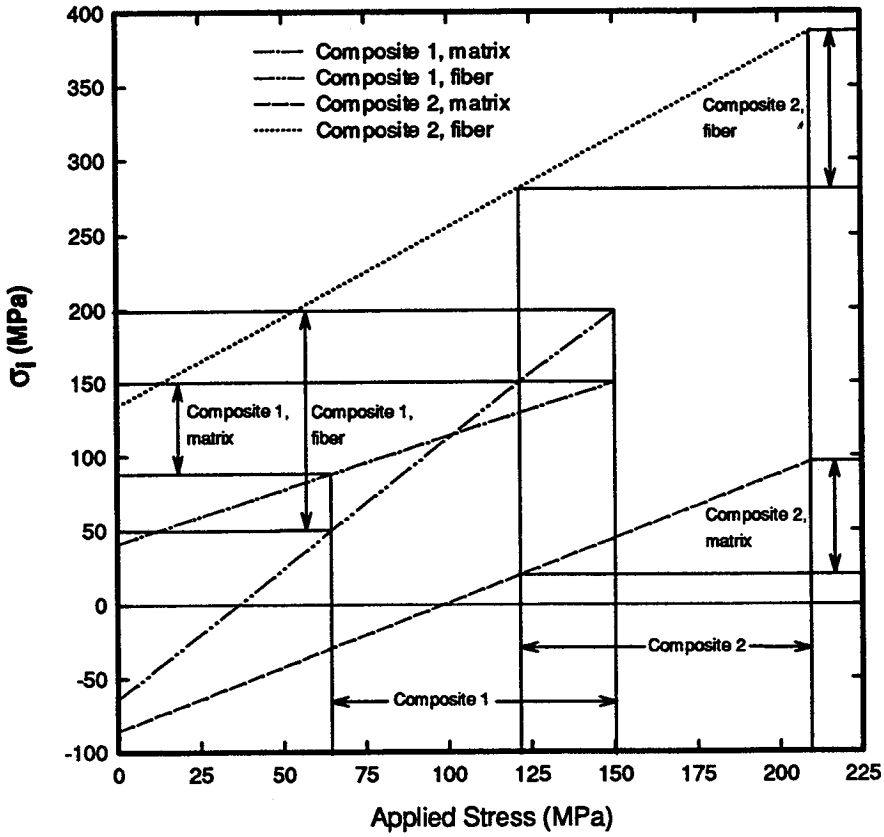

Figure 23 Schematic showing the stresses in fibers and matrix, σ_i, where i = z = load direction, r = radial direction or θ = circumferential direction as calculated by a thermoelastic concentric cylinder model for SiC/CAS[0°] and SiC/MAS-5[0°], at 600°C.

Analyses for this paper were done only for the glass-ceramic unidirectionally-reinforced composites because they were the easiest to analyze because a concentric cylinder model could be readily used and compared to the TMF life results. Also, the porosity was much smaller than the fiber diameters thereby having less of an effect on TMF behavior than was in the SiC/SiC composites where the pores were relatively large. Also few data points were collected for the enhanced SiC/SiC. The relatively flat life versus maximum cyclic stress curves of Figs. 10 & 11 for SiC/CAS and SiC/MAS-5 suggested that there existed a critical stress state. At this stress level, crack propagation initiated at a significant enough level to cause failure in less than 1000 cycles. Any higher cyclic stress level led to a dramatic drop in TMF life (relatively flat stress-life plot). For these reasons an equation that predicts the life up to 1000 cycles is practically useless.

A model that assumes axisymmetry in the stress states in the fibers and matrix was used [12]. This was done for the maximum applied stress in the TMF and isothermal fatigue cycles using the thermoelastic properties of the fibers and matrix from Table I. In these calculations, z is in the load and fiber axis direction, r is in the radial direction, and θ is in the circumferential direction. The circumferential direction is with respect to the cross-section of the fibers. In presenting the results of the analysis, the stresses in the matrix and fibers will be presented as a function of applied stress at the lower temperature of 600°C. This was done because these composites failed at the location close to this temperature simultaneous with the maximum cyclic applied stress. The assumption is that the damage is determined by the stress states in the fiber and matrix at maximum applied stress.

Figure 23 shows schematically how the results of the analysis are presented. The figure shows the stresses in the load direction (z) in the fibers and matrix at 600°C as a function of applied stress in the load direction. For each of the two composites drop lines are drawn from along the applied stress axis up to each of the plots for the fiber and matrix of each composite. The value of applied stress at the intersection of the axis and drop line represents the value of maximum cyclic stress where the TMF lives are approximately 1000 cycles (left drop line) and where the composite survived less than 10

cycles (right drop line). The drop lines to the left and right provide the values of stress in the fiber and matrix of the two composites, respectively.

Figure 24 shows the stresses in the load direction (z) in the fibers and matrix at 600°C for the unidirectionally reinforced CAS and MAS-5 matrix composites, respectively. For the SiC/CAS the drop lines range from 65 MPa to 150 MPa. The σ_z in the matrix ranges from about 88 MPa to 150 MPa, respectively, and for the fibers, ranges from about 29 MPa to 151 MPa. As noted on the left vertical axis, the stress in the matrix at room temperature and zero stress is 85 MPa. This value is approximately equal to the stress in the matrix at 600°C and 65 MPa applied stress. Recalling Fig. 10(a) this composite in OP TMF experienced a dramatic decrease in TMF life at this applied stress level (falling from about 1000 cycles to less than 20 cycles). An explanation for the OP TMF behavior of the SiC/CAS[0°] might be that during cooldown from processing the matrix developed the residual stress of 85 MPa at room temperature. This residual stress may have caused some microcracking of the matrix that could not be seen at zero load because they closed tightly. Upon loading in OP TMF at a maximum cyclic stress of 65 MPa the stress in the matrix just began to exceed the residual stress value of 85 MPa at room temperature. As a result the cracks were opened and propagated further and also caused residual crack opening displacements because of the frictional sliding and interlocking at the interface during cyclic loading. As the cracks developed, the load was transferred to the fibers. Subsequently, oxygen could penetrate to these regions of the fibers, causing bonding of the matrix to the fibers, so failure of the fibers was facilitated.

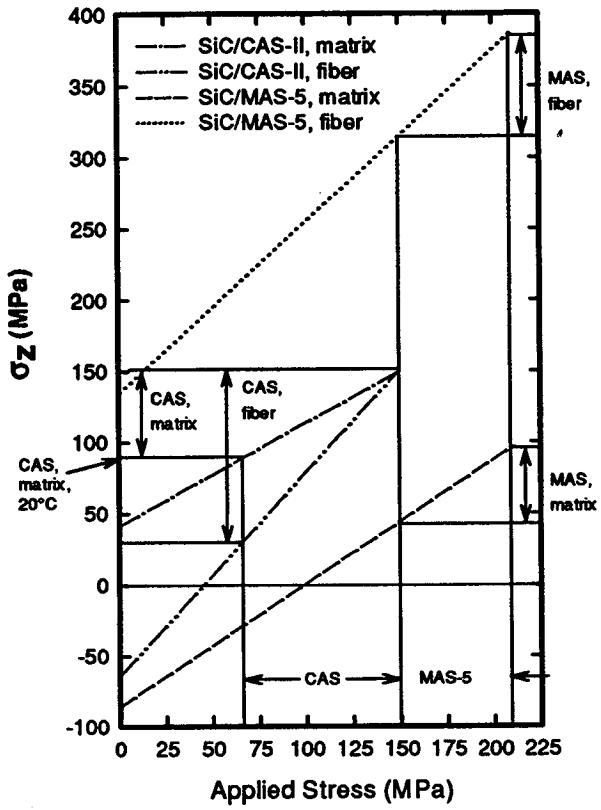

Figure 24 Stresses in fibers and matrix in the load direction σ_z as calculated by a thermoelastic concentric cylinder model for SiC/CAS[0°] and SiC/MAS-5[0°], at 600°C.

In contrast, for the SiC/MAS-5[0°] composite, the range of maximum cyclic stresses was from 150 to 210 MPa over the same range of OP TMF lives. Over this range the stress in the matrix ranged from about 44 MPa to about 97 MPa. These values are lower than those for SiC/CAS[0°] which is of interest since the fracture toughnesses of the two matrices are expected to be about the same. However, the differences in the matrix cracking stress values may be explained by the difference in radial stresses. Fig. 25 shows that σ_r is relatively insensitive to applied stress at a particular temperature. In the SiC/MAS-5[0°] the residual radial stress of about 60 MPa is tensile compared to a compression value of 25 MPa in the SiC/CAS[0°]. Residual tensile stress at the interface facilitates debonding and separation of fiber and matrix at the debond thereby decreasing the frictional or interlocking shear stresses at the interface. The result is lower matrix-crack closure loads due to fiber bridging causing a lower matrix cracking stress. Of course the applied stress is much higher in the SiC/MAS-5[0°] because the CTE of the matrix is less than that of the fiber, opposite to that of the SiC/CAS[0°] composite.

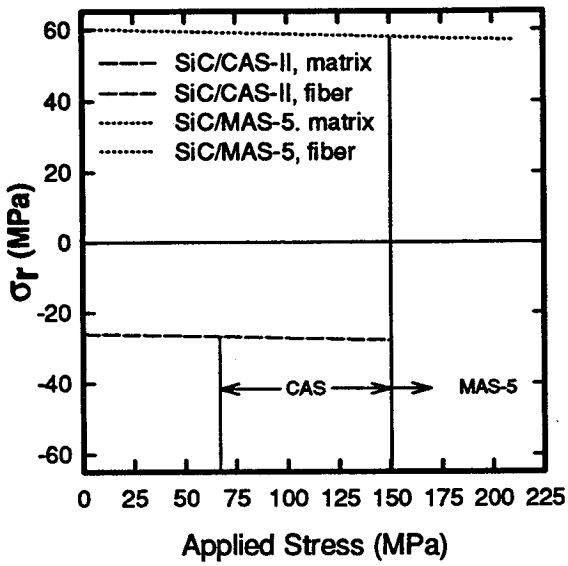

Figure 25 Stresses in fibers and matrix in the radial direction σ_r as calculated by a thermoelastic concentric cylinder model for SiC/CAS[0°] and SiC/MAS-5[0°] at 600°C.

Another important difference between the two composites in Fig. 24 for OP TMF is that the stress in the fibers of the SiC/MAS-5[0°] is much higher than in the SiC/CAS[0°]. Since the fiber volume fractions are the same, (load shedding to fibers roughly in proportion as a result of matrix cracking) this difference would be expected to be maintained during TMF cycling. An explanation may be that the wide crack opening displacements during OP TMF may allow rapid oxidation of the fibers and interface. There would be a subsequent loss of strength of the fibers to occur that the difference in stress values may be of minimal importance.

The results of Figs 24 and 25 would explain why the IP specimens failed in the transition region near 600° while the gage is near 1100°C. This is accounted for by the fact that creep deformation was occurring in the IP specimens around the maximum temperature of 1100°C. There are no published values of creep of these two neat matrices, especially at the conditions of interest. The author has performed some 4 pt. bend creep experiments of the two neat matrices in the 900°C to 1100°C range. The trend of the results indicated a creep threshold for glass-ceramics in about the 850°C-900°C range. It was found that the CAS-II creeps at a much faster rate than the MAS neat matrix. The Nicalon™ fiber has a creep threshold of approximately 1000°C [13,14], so both the fiber and matrix are expected to creep at 1100°C. In all the IP tests performed that lasted longer than about 10 cycles strain ratcheting was experienced. It appears that creep deformation had retarded matrix cracking in the gage section, whereas in the transition region microcracking occurred below the creep threshold temperature. At this area in the transition region, the carbon interface would have still oxidized away leading to embrittlement of the composite.

The analysis and discussion of the analysis are consistent with the experimental results. OP specimens failed near or in the gage section around 600°C at a stress that initiated microcracking of the matrix. Rapid oxidation led to failure. In the IP specimens, failure also occurred in the region of the specimen where the temperature was 600°C or a little higher while the applied stress was maximum. Creep deformation in regions of higher temperature retarded cracking and oxidation. In the OP specimens, the location of matrix cracking cycles between approximately 600° and 1100°C. This produced faster oxidation embrittlement of the composite compared to the failure location in the IP specimens where the maximum temperature was 600°-700°C. This explained why the maximum cyclic applied stresses were higher for the IP specimens than the OP specimens for the same TMF lives. Therefore, it appears that for CFCC's a potential limiting factor is the combination of brittleness and oxidation at intermediate temperatures. Interface materials must be found that are more oxidation resistant to higher temperatures than carbon.

Thermal gradients may have influenced the failure locations because any microcracking would have allowed oxidation embrittlement of the composite. If the composites were not sensitive to oxidation and as result retained psuedo-ductility due to fiber bridging and interface sliding, they would have been expected to experience failures in the gage section. This is because the nominal direct stress was maximum in the gage section.

The failure initiation sites in the glass-ceramic matrix composites were not positively identified. However, using a fracture toughness value of 2 MPa-$m^{½}$ [11,16] for the neat glass-ceramic matrices and a stress of about 90 MPa, the size of the initiating flaws would have been in the 100-200 micron size range. Examining Fig. 5(a) and (b), 100-200 microns corresponds to approximately the areas where the fibers clumped together with uninfiltrated areas around them.

Summary

Three fiber-reinforced ceramics with varying matrices and fiber architectures were tested under TMF conditions. Microstructural examination of failed specimens was conducted to provide insight into the damage mechanisms and factors determining TMF lives.

1. The SiC/SiC[PW] without a matrix enhanced for oxidation resistance had the shortest TMF lives of the composites tested and the enhanced SiC/SiC[PW] had the longest. The SiC/MAS-5[0°] had longer TMF lives than the SiC/CAS[0°].

2. In all the composites tested OP TMF was worse than IP TMF. The difference between the two was greatest for the SiC/CAS[0°] and least for the SiC/SiC[PW].

3. TMF lives were shorter than for isothermal fatigue, creep, or thermal cycling with a static load.

4. TMF failure in the SiC/CAS[0°] was not achieved in an argon environment at maximum cyclic stress levels at least double those in the air tests. Oxidation is a dominant factor in the TMF behavior of these CFCC's.

5. The applied maximum cyclic stress for unidirectional SiC/MAS-5 was twice that of the cross-ply for the same TMF life.

6. TMF lives of 35 ply and 18 ply thick specimens of SiC/CAS[0°] were similar.

7. During IP TMF, primary strain ratcheting was experienced throughout the tests. In OP tests the maximum and minimum strains were essentially constant. There does not appear to be a correlation between total strain to failure between different maximum cyclic stress levels.

8. Under OP and IP TMF the SiC/CAS and SiC/MAS-5 composites failed by transverse cracking of the matrix from the edge of the specimens. However, in the OP tests there was significant fiber failure in the plane of the matrix crack with a large residual crack opening displacement. In the IP tests the matrix cracks were fully bridged by fibers. In IP tests there was evidence of more fiber pullout on the fracture surfaces than the OP tests.

9. Failures at least for the glass-ceramic matrix composites occurred at the location of the maximum stress and temperature of about 600°-700°. In the OP specimens this location was near or within the gage section. In the IP specimens this location was further into the transition region.

10. A preliminary analysis of the stresses in the fibers and matrices accounted for their respective thermoelastic properties. The results implied that the failures were caused by matrix cracking followed by penetration of oxygen to the fibers on the crack plane in the specimen. The higher stress concentration and degradation by oxidation of the fibers on the crack plane caused sudden catastrophic failure on that plane. In the IP case, creep of the matrix and fibers within the gage section retarded crack formation thus inhibiting oxidation embrittlement in the gage section. Therefore, the glass-ceramic matrix composites tested have an intermediate temperature problem of brittleness and oxidation. The carbon interface was surmised to be the main problem.

Conclusions

The TMF behavior of these three fiber-reinforced ceramics was the result of the particular thermomechanical properties of the constituents. The relative response to in-phase TMF and out-of-phase TMF was a function of properties such as the different coefficients of thermal expansion, elastic moduli, creep, and fracture toughnesses of the fiber and matrices. The damage mechanisms for each type of thermomechanical cycling were the result of each of these factors during each loading condition.

TMF testing provides not only a test that evaluates the CFCC's behavior under prototypical load conditions but also provides a "screening test" early in the evaluation process of particular composite systems. The claim that TMF testing is too slow and complicated is countered by the fact that previous TMF testing on CFCC's provides a "reference point" for rapid comparison. Relatively few OP TMF tests can be performed for a direct comparison with other CFCC's. Any significant improvement in composite performance can be readily determined. Simultaneously, a preliminary evaluation of the composites' suitability for applications is accomplished. Also, since many applications involve components subject to startup and shutdown cycles and with hold times at temperature and load, TMF testing with hold times provides a more realistic evaluation. The startup and shutdown cycles force the composites into a transient state for a large percentage of the use time. TMF testing is ideal to simulate this condition..

Failure location in a properly designed specimen provides a realistic evaluation of the performance of the composite under prototypical loading conditions and should be reported for this class of composites.

The main barrier to use of these composites at least for the glass-ceramic matrix composites is the intermediate temperature problem of brittleness and oxidation. Replacements must be found for the carbon interface.

Acknowledgements

I wish to acknowledge the assistance of John Miller and Chris Burke with the mechanical, and Ron Shinn with the electronic aspects of the experimental equipment. Also I thank Patricia Dickerson for producing the SEM micrographs and Michael Miller and Todd Leonhardt for preparing the polished ceramographic cross-sections from the composites.

References

1. Castelli, M.G.; Ellis, J.R.; and Bartolotta, P.A.: Thermomechanical Testing Techniques for High-Temperature Composites: TMF Behavior of SiC(SCS-6)/Ti-15-3. NASA TM-103171, 1990.
2. Verrilli, M.J.; and Bartolotta, P.A.: Thermomechanical Fatigue of Metal Matrix Composites: Status Report from the 6th Thermomechanical Fatigue Workshop, HITEMP Review 1991: Advanced High Temperature Engine Materials Technology Program, NASA CP-10082, 1991, pp. 48-1 to 48-12.
3. Butkus, L.M.: Thermomechanical Fatigue Behavior of a Silicon Carbide Fiber-Reinforced Calcium Aluminosilicate Glass-Ceramic Matrix Composite. M.S. Thesis, University of Michigan, 1991.

4. Worthem, D.W.: Flat Tensile Specimen Design for Advanced Composites. NASA CR-18561, 1990.
5. Pluvinage, P., Kuo, W.-S., Parvizi-Majidi, A. and Chou, T.-W.: Damage Mechanics and Mechanisms in SiC/SiC Composites, HITEMP Review 1992: Advanced High Temperature Engine Materials Technology Program, NASA CP-10104, 1992, pp. 67-1 to 67-16.
6. Rice, R.W.: Pores as fracture origins in ceramics. Journal of Materials Science, vol. 19, 1984, pp. 895-914.
7. Pryce, A.W.; and Smith, P.A.: Behaviour of unidirectional and crossply ceramic matrix composites under quasi-static tensile loading. Journal of Materials Science, vol. 27, 1992, pp. 2695-2704.
8. Worthem, D.W.; and Lewinsohn, C.A.: Effect of Specimen Design on the Tensile Properties of Ceramic Matrix Composites, HITEMP Review 1991: Advanced High Temperature Engine Materials Technology Program, NASA CP-10082, 1991, pp. 49-1 to 49-10.
9. Zawada, L.P., unpublished data.
10. Castelli, M.G., An Advanced Test Technique to Quantify Thermomechanical Fatigue Damage Accumulation in Composite Materials, Journal of Composites Technology and Research, to appear, Oct., 1994.
11. Marshall, D.B.; and Evans, A.G.: Failure Mechanisms in Ceramic-Fiber/Ceramic-Matrix Composites. J. Am. Ceram. Soc., vol. 68, no.5, 1985, pp. 225-231.
12. Hecker, S.S.; Hamilton, C.H.; and Ebert, L.J.: Elastoplastic Analysis of Residual Stresses and Axial Loading in Composite Cylinders: Journal of Materials, JMLSA, vol. 5, no. 4, 1970, pp. 868-900.
13. Simon, G., Bunsell, A. R., Mechanical and structural characterization of the Nicalon silicon carbide fibre. Journal of Materials Science, vol. 19, 1984, pp. 3649-3657.
14. DiCarlo, J.A., Morscher, G. N.: Creep and Stress Relaxation Modeling of Polycrystalline Ceramic Fibers: in "Failure Mechanisms in High Temperature Composite Materials", eds. Haritos, G.K. et al., AD-Vol. 22, AMD-Vol. 122, ASME, New York, 1991, pp. 15-22.
15. Frety, N.; Molins, R; Broussuge, M.: Oxidizing ageing effects on SiC-SiC composites: Journal of Materials Science, vol. 27, 1992, pp. 5084-90.
16. Evans, A.G.: The Mechanical Performance of Fiber-reinforced Ceramic Matrix Composites: Materials Science and Engineering, vol. A107, 1989, pp. 227-39.

Appendix

(For the failure locations, U = upper half and L= lower half of specimens, G = within gage section.)

TABLE A.1-SUMMARY OF DATA FOR SiC/CAS[0°]$_{35}$

{Air environment except where noted}

Specimen I.D.	Type of Test	Maximum stress, MPa	Cycles to failure, N_f or to interruption ("N_I=")	Failure location, distance from center, mm	Temp, (°C) at failure location when gage section at 1100°-600°C	Nominal stress (MPa) in loading direction at failure location, (%) of gage section stress
8916006L-2	IP	74	N_I= 10,176	-	-	-
-3	IP	150	77	L, 33.5	663-391	91
-4	IP	150	73	L, 32.0	704-410	92
-5	IP	125	1313	L, 32.9	679-399	91
-6	IP	125	748	L, 32.9	679-399	91
-7	OP	150	6	L, 16.0	1067-580	100
-8	OP	125	8	L, 19.0	1056-571	99
-9	OP	100	18	L, 17.2	1062-576	100
-10	OP	72	18	GL, 2.9	1097-600	100
8931003L-1	IP	119.4	2518	L, 38.9	517-324	86
-2	ISO, 600°C	150	N_I= 1056	-	-	-
-3	ISO, 1100°C	150	264	L, 31.5	717	92
-4	ISO, 1100°C	136.8	N_I= 2005	-	-	-
-5	Creep, 1100° C	150	254*	L, 22.5	961	98
-7 (argon)	IP	275	N_I= 1002	-	-	-
-8 (argon)	OP	250	N_I= 1000	-	-	-
-9	OP	50	N_I= 1039	-	-	-
-10	OP	60	N_I= 364	-	-	-

* Equivalent number of cycles based on a 6 minute cycle time.

TABLE A.2-SUMMARY OF DATA FOR SiC/CAS[0°]$_{18}$

{Air environment}

Specimen ID	Type of Test	Maximum stress, MPa	Cycles to failure, N_f or to interruption ("N_I=")	Failure location, distance from center, mm	Temp, (°C) at failure location when gage section at 1100°-600°C	Nominal stress (MPa) in loading direction at failure location, (%) of gage section stress
9220901L-1	IP	150	60	L, 31.1	728-421	91
-7	IP	125	N_I= 3054	-	-	-
-8	OP	80	16	GU, 6.4	1093-600	100
-9	OP	65	252	L, 7.9	1092-600	100
-10	OP	65	577	L, 29.3	777-443	93
-11	IP	150	6	L, 29.0	785-447	93
9220902L-1	IP	150	27	L, 35.0	622-373	88
-2	IP	125	N_I= 3155	-	-	-
-3	IP	150	15	U, 32.5	690-404	90
-4	OP	125	4	GU, 3.6	1096-600	100
-5	OP	125	5	U, 13.6	1075-587	100
-6	OP	70	225	U, 31.4	720-417	91
-7	OP	95	17	U, 30.0	758-434	92
-8	OP	80	16	GU, 6.4	1093-600	100
-9	OP	65	71	L, 28.5	799-453	93

TABLE A.3-SUMMARY OF DATA FOR SiC/MAS-5[0°]$_{16}$

{Air environment}

Specimen ID	Type of Test	Maximum stress, MPa	Cycles to failure, N_f or to interruption ("N_I=")	Failure location, distance from center, mm	Temp, (°C) at failure location when gage section at 1100°-600°C	Nominal stress (MPa) in loading direction at failure location, (%) of gage section stress
9307401L-2	OP	150	N_I= 1060	-	-	-
-3	OP	210	8	GL, 3.2	1097-600	100
-4	OP	175	40	GU, 0.7	1100-600	100
-5	IP	150	N_I= 1003	-	-	-
-6	IP	175	N_I= 1072	-	-	-
-7	IP	210	359	U, 35.7	604-364	87
9307403L-1	CS, 600°-1100°C	175	N_I= 1780	-	-	-
-2	OP	175	19	GU, 6.8	1093-600	100
-3	OP	165	17	GL, 1.8	1098-600	100
-4	OP	155	192	L, 22.5	961-527	97
-5	OP	150	679	GU, 3.2	1097-600	100
-6	ISO, 23°C	210	N_I= 1100	-	-	-
-7	CS, 600°-1100°C	210	861	U, 34.6 & L, 33.9	663-377 & 652-386	88 & 89
-9	IP	210	32	L, 34.5	636-379	88
-10	CS, 600°-1100°C	210	631	U, 34.2 & L, 33.2	644-382 & 671-395	89 & 90

TABLE A.4-SUMMARY OF DATA FOR SiC/MAS-5[0°/90°]$_{8S}$

{Air environment}

Specimen ID	Type of Test	Maximum stress, MPa	Cycles to failure, N_f or to interruption ("N_I=")	Failure location, distance from center, mm	Temp, (°C) at failure location when gage section at 1100°-600°C	Nominal stress (MPa) in loading direction at failure location, (%) of gage section stress
9307404L-1	OP	150	1	U, 19.3	1048-567	98
-2	OP	100	4	L, 12.1	1081-592	100
-3	OP	75	N_I= 1211	-	-	-
-4	IP	150	2	U, 13.2	1077-589	100
-5	IP	125	13	L, 16.4	1065-579	99
-6	IP	100	N_I= 1038	-	-	-

TABLE A.5-SUMMARY OF DATA FOR SiC/SiC[PW]$_{12}$

{Air environment}

Specimen ID	Type of Test	Maximum stress, MPa	Cycles to failure, N_f or to interruption ("N_I=")	Failure location, distance from center, mm	Temp, (°C) at failure location when gage section at 1100°-600°C	Nominal stress (MPa) in loading direction at failure location, (%) of gage section stress
516636-1	IP	65	128	U, 18.0	1059-574	99
-2	IP	60	114	U, 26.4	855-479	95
-3	IP	55	313	L, 23.2	942-519	97
-4	IP	50	82	L, 14.8	1071-584	100
-5	IP	50	N_I= 1315	-	-	-
-6	OP	40	288	L, 19.0	1056-571	98
-7	OP	30	N_I= 1515	-	-	-
-8	ISO, 1100° C	65	34	U, 20.4	1018	98
-9	ISO, 1100° C	50	654	L, 24.6	904	96
-10	ISO, 850° C	65	208	U, 12.0	838	100
-11	ISO, 600° C	65	N_I= 1060	-	-	-
-12	ISO, 1000° C	65	84	U, 20.4	922	98
-13	IP	75	47	U, 19.0	1056-571	98
-14	Creep, 1100° C	65	16*	GL, 3.5	1096	100
-15	Creep, 1100° C	50	513*	U, 24.6	904	96
-16	OP	75	36	U, 14.1	1073-586	100
-17	OP	75	43	GL, 6.3	1093-600	100
516638-13	OP	65	42	U, 15.0	1070-583	100
-14	OP	50	209	L, 19.7	1037-562	98
-15	IP	50	N_I= 1034	-	-	-

TABLE A.6-SUMMARY OF DATA FOR ENHANCED SiC/SiC[PW]$_{12}$

{Air environment}

Specimen ID	Type of Test	Maximum stress, MPa	Cycles to failure N_f, or to interruption ("N_I=")	Failure location, distance from center, mm	Temp, (°C) at failure location when gage section at 1100°-600°C	Nominal stress (MPa) in loading direction at failure location, (%) of gage section stress
ENH1-2	OP	85	1130	GU, 7.0	1093	100
-3	OP	150	88	GU, 19.9	1047	100
-4	OP	125	133	GU, 8.8	1091	100
-5	OP	100	364	U, 23.5	950	96
-6	IP	100	886	U, 21.5	1004	99

REPORT DOCUMENTATION PAGE

Form Approved
OMB No. 0704-0188

Public reporting burden for this collection of information is estimated to average 1 hour per response, including the time for reviewing instructions, searching existing data sources, gathering and maintaining the data needed, and completing and reviewing the collection of information. Send comments regarding this burden estimate or any other aspect of this collection of information, including suggestions for reducing this burden, to Washington Headquarters Services, Directorate for Information Operations and Reports, 1215 Jefferson Davis Highway, Suite 1204, Arlington, VA 22202-4302, and to the Office of Management and Budget, Paperwork Reduction Project (0704-0188), Washington, DC 20503.

1. AGENCY USE ONLY (*Leave blank*)	2. REPORT DATE	3. REPORT TYPE AND DATES COVERED
	March 1995	Final Contractor Report

4. TITLE AND SUBTITLE
Thermomechanical Fatigue Behavior of Three CFCC's

5. FUNDING NUMBERS
WU–505–63–5B
C–NAS3–25266

6. AUTHOR(S)
Dennis W. Worthem

7. PERFORMING ORGANIZATION NAME(S) AND ADDRESS(ES)
NYMA, Inc.
Engineering Services Division
2001 Aerospace Parkway
Brook Park, Ohio 44142

8. PERFORMING ORGANIZATION REPORT NUMBER
E–9484

9. SPONSORING/MONITORING AGENCY NAME(S) AND ADDRESS(ES)
National Aeronautics and Space Administration
Lewis Research Center
Cleveland, Ohio 44135–3191

10. SPONSORING/MONITORING AGENCY REPORT NUMBER
NASA CR–195441

11. SUPPLEMENTARY NOTES
Work performed when author was with Sverdrup Technology Inc. Project manager, Brad Lerch, Structures Division, NASA Lewis Research Center, organization code 5220, (216) 433–5522.

12a. DISTRIBUTION/AVAILABILITY STATEMENT
Unclassified - Unlimited
Subject Category 24

This publication is available from the NASA Center for Aerospace Information, (301) 621–0390.

12b. DISTRIBUTION CODE

13. ABSTRACT ***(Maximum 200 words)***

The thermomechanical fatigue (TMF) behavior of three continuous-fiber ceramic composites (CFCC's) was examined. The three matrices consisted of two different glass-ceramics and silicon carbide, respectively. The matrices of some of the specimens with the silicon carbide matrix were enhanced to improve oxidation resistance. All three were reinforced with Nicalon^{TM} fibers with various fiber architectures. The thermoelastic properties of the matrix relative to the fibers, the elastic moduli and coefficients of thermal expansion (CTE), were different in each composite, providing a comparison of the effects of these critical properties. The specimens were tested under in-phase (IP) and out-of-phase (OP) cyclic loadings with respect to thermal cycling between 600°C and 1100°C. One of the glass-ceramic composites had greatly increased TMF lives compared to the other glass-ceramic matrix composite. This was probably caused by the reversal of the CTE mismatch between the fibers and the matrices and caused by the different oxidation resistances of the composites. For the same TMF lives a cross-ply reinforced composite had a maximum cyclic stress half as great, as that of unidirectionally reinforced composite. This indicated that the [0°] ply fibers had a strong influence on TMF life. Both the glass ceramic matrix composites had shallow-slope stress-life plots that indicated sensitivity to damage and therefore low damage tolerance. The composites with an unenhanced silicon carbide martix experienced the shortest TMF lives of all the CFCC's tested. However the enhanced composite had the longest. Also, the enhanced composite demonstrated the best damage tolerance as evidenced by a stress-life curve that curves sharply upward to the left. In all the composites, out-of phase cyclic loading was worse than in-phase cyclic loadings despite the CTE mismatch between fiber and matrix. A damage investigation and a preliminary analysis of the stresses in the fibers and matrices taking into account their respective thermoelastic properties provided insight into the relative behavior of the glass-ceramic matrix composites under IP and OP TMF.

14. SUBJECT TERMS
Continuous fiber-reinforced ceramics-(CFCC's); Ceramic matrix composites(CMC's); Fatigue; Thermomechanical fatigue (TMF); Creep; Isothermal; Calcium aluminosilicate; Magnesium aluminosilicate; Glass-ceramics; Silicon carbide; Fibers; Matrix; Fiber pullout; Failure; Coefficient of thermal expansion; Elastic moduli; Mismatch

15. NUMBER OF PAGES
25

16. PRICE CODE
A03

17. SECURITY CLASSIFICATION OF REPORT	18. SECURITY CLASSIFICATION OF THIS PAGE	19. SECURITY CLASSIFICATION OF ABSTRACT	20. LIMITATION OF ABSTRACT
Unclassified	Unclassified	Unclassified	